Personalized Biopsy Schedules Using an Interval-censored Cause-specific Joint Model

Zhenwei Yang[1,2], Dimitris Rizopoulos[1,2], Eveline A.M. Heijnsdijk[3], Lisa F. Newcomb[4], and Nicole S. Erler[1,2]

[1]Department of Biostatistics, Erasmus Medical Center Rotterdam
[2]Department of Epidemiology, Erasmus Medical Center Rotterdam
[3]Department of Public Health, Erasmus Medical Center Rotterdam
[4]Fred Hutchinson Cancer Research Center, Cancer Prevention Program, Public Health Sciences, Seattle, Washington

January 3, 2023

Abstract

Active surveillance (AS), where biopsies are conducted to detect cancer progression, has been acknowledged as an efficient way to reduce the overtreatment of prostate cancer. Most AS cohorts use fixed biopsy schedules for all patients. However, the ideal test frequency remains unknown, and the routine use of such invasive tests burdens the patients. An emerging idea is to generate personalized biopsy schedules based on each patient's progression-specific risk. To achieve that, we propose the interval-censored cause-specific joint model (ICJM), which models the impact of longitudinal biomarkers on cancer progression while considering the competing event of early treatment initiation. The underlying likelihood function incorporates the interval-censoring of cancer progression, the competing risk of treatment, and the uncertainty about whether cancer progression occurred since the last biopsy in patients that are right-censored or experience the competing event. The model can produce patient-specific risk profiles until a horizon time. If the risk exceeds a certain threshold, a biopsy is conducted. The optimal threshold can be chosen by balancing two indicators of the biopsy schedules: the expected number of biopsies and expected delay in detection of cancer progression. A simulation study showed that our personalized schedules could considerably reduce the number of biopsies per patient by 34%-54% compared to the fixed schedules, though at the cost of a slightly longer detection delay.

Keywords: Competing Risk; Dynamic Prediction; Interval Censoring; Joint Models; Precision Medicine

1 Introduction

Prostate cancer is the most frequently diagnosed and the second most commonly occurring cancer in men worldwide (Gandaglia et al., 2021). However, most cases are indolent and immediate treatment is usually unnecessary (Pernar et al., 2018; Albertsen et al., 2005). An analysis of the Medicare and Surveillance, Epidemiology and End Results (SEER) dataset estimated an overtreatment rate of 67% in low-risk patients with prostate cancer (Aizer et al., 2015). Since active surveillance (AS) has been widely acknowledged as an efficient way to reduce overtreatment (Chen et al., 2016), a consensus has been reached that low-risk patients should enter AS and defer treatment until the confirmation of cancer progression.

There exist several AS protocols implemented in different countries. The majority of the existing AS cohorts used fixed biopsy schedules for all patients, with frequencies ranging from every one to four years (Bul et al., 2013; Tosoian et al., 2011; Klotz et al., 2015; Welty et al., 2015; Adamy et al., 2011; Davis et al., 2016; Newcomb et al., 2016; Godtman et al., 2016; Selvadurai et al., 2013; Lowenstein et al., 2019). However, due to the lack of evidence for the ideal test interval, the discussion about biopsy schedules is still ongoing (Bruinsma et al., 2016). The tumor status of the patients in AS is monitored by related biomarkers, such as

the prostate-specific antigen (PSA) level, as well as repeated biopsies. Dall'Era et al. (2008) reported a cancer progression rate of 31% in AS, indicating that most patients regularly undergo unnecessary examinations. A particular difficulty in determining an appropriate frequency for regular biopsies is that frequent biopsies are associated with an increased patient burden and risk for complications. In contrast, infrequent biopsies increase the chance of cancer progression being missed, resulting in more adverse clinical outcomes. Biopsy schedules that safely relieve the burden of frequent biopsies and balance the harms and benefits are needed. To that effect, we argue that biopsy schedules should be customized based on the individuals' risk.

Although such personalized AS schedules are not yet implemented in prostate cancer, different studies have proposed methodologies for individualized cancer surveillance. Zhou et al. (2020) elaborated on selecting the nasopharyngeal carcinoma posttreatment surveillance strategies from a pool of schedule candidates constructed according to the time-specific occurrence probabilities for the time to disease recurrence derived from a random survival forest. They selected the optimal personalized schedule as the most cost-effective one in the simulation from a Markov model. However, their model only distinguished between different risk groups and not individual patients. Moreover, the model described by Zhou et al. (2020) can handle right censored survival data (Ishwaran et al., 2008), whereas an additional challenge in cancer AS is that, due to the periodical examinations, the time of progression is not observed exactly, resulting in interval censoring. Despite the limited literature discussing ideas of scheduling, recent studies focus on the risk models that can serve for the decision-making process (e.g., Mamawala et al., 2017; Nayan et al., 2022; Eminaga et al., 2022). One recent paper proposed a new model for the individual's risk of cancer progression employing a deep learning technique, the Dynamic-DeepHit-Lite model (Lee et al., 2022). The model also included the longitudinal trajectory of the PSA, which is believed to be a sensitive biomarker for prostate cancer (Cary and Cooperberg, 2013). Generally, in the observed data, repeated biomarker measurements require special caution since they are typically endogenous and likely affected by measurement error.

So far, only Tomer et al. (2019, 2022) proposed a methodology for prostate cancer AS that can handle the biomarkers' dynamic nature, endogeneity, and measurement error, as well as the interval-censoring of the event of interest. The authors used a joint model for longitudinal and time-to-event data, in which the risk of cancer progression was derived from each patient's trajectories of the biomarkers over time, and is thus patient-specific. Nonetheless, these authors did not consider the informative censoring due to an early initiation of treatment. Typically a patient's decision to leave AS to seek treatment is associated with his (perceived) risk of progression and initiating treatment changes this risk. In the Canary Prostate Active Surveillance Study (PASS) that motivates our work, around 10% of the participants initiated treatment before cancer progression had been detected (Cooperberg et al., 2020). The failure to account for the competing risks can bias the estimated cumulative risk of progression and eventually mislead the decision-making for personalized schedules (Schuster et al., 2020).

Our current study aims to extend the model and theoretical framework for personalized biopsy schedules proposed by Tomer et al. (2022) to a setting with both interval-censoring and competing risks. Different events may have different censoring patterns (i.e., the time of progression is interval censored; the time of treatment initiation is exactly observed). Consequently, the censoring times may differ per event type: while the time to treatment initiation is censored when a patient leaves AS for another reason, the time to cancer progression for the same patient is censored at the last available biopsy. To overcome this challenge while also considering the aforementioned dynamic nature of (endogenous) biomarkers that may be measured with error, we develop an interval-censored cause-specific joint model (ICJM) that combines a cause-specific proportional hazard model with a multivariate mixed model. Our model incorporates the "core ratio" as an additional biomarker to improve the precision of the risk of progression. The "core ratio" denotes the proportion of samples taken during a biopsy that contain cancer cells. A particular feature that needs consideration is that since the core ratio is obtained in each biopsy, measurement times generally differ from the times at which PSA measurements are taken.

Using the ICJM, we also extend the methodology to create personalized biopsy schedules previously proposed by Tomer et al. (2022) to a setting with competing events. Biopsies are scheduled when the estimated individual progression-specific risk, derived from the ICJM, exceeds a certain threshold. Under the assumption that the scheduled biopsy indicates absence of progression, the risk is reset to zero at that time, and the subsequent biopsy can be planned in the same manner. Different choices of thresholds will result in different numbers of planned biopsies (fewer seen as benefits) and different detection delays (longer seen as harm). To further tailor the schedules to each patient's risk profile, we determine patient-specific

thresholds by balancing the two indicators for each patient. Schedules can be dynamically updated whenever additional information on the biomarkers becomes available.

The remainder of this paper is organized as follows. In Section 2, we describe the motivating Canary PASS data. Section 3 defines the proposed interval-censored cause-specific joint model, and the personalized scheduling strategy is elaborated in Section 4. The results from two ICJMs fitted on Canary PASS data are presented in Section 5. Section 6 presents a simulation study to compare our personalized schedules with the existing fixed schedules for biopsies in AS. Section 7 concludes this paper with a discussion.

2 Canary PASS Data

The Canary PASS trial is an ongoing multicenter active surveillance study in the US (Newcomb et al., 2016). Patients are monitored with PSA tests every three months, clinical visits every six months, and biopsies at 12, 24 months, and biennially afterwards. The biopsies determine the tumor status, which is reflected in the Gleason score. In 2017, the trial included 850 patients diagnosed since 2003 with a Gleason score of six, who were found with a Gleason score of six or no cancer on confirmatory biopsy (Cooperberg et al., 2020). Our current study includes 833 subjects with at least one PSA value recorded while on AS. The primary outcome, cancer progression, is defined as a Gleason score of seven or higher. Patients who reach this endpoint leave AS to receive treatment. Notably, 87 patients left AS for treatment before cancer progression was detected, constituting the competing event. The summary of the data is presented in Web Appendix A.1.

Previous research has shown that the level of PSA, as well as the velocity of PSA level change, are predictive of cancer progression (Nelson et al., 2021; Cary and Cooperberg, 2013). Previous knowledge about the association may induce patients to start early treatment when they see increasing PSA values. Hence, our aim here is to model the relation between PSA and cancer progression while considering the competing risk and to obtain risk estimates from this model that allow us to generate risk-based biopsy schedules. Furthermore, we also explore using another clinically relevant biomarker, the core ratio, as an additional time-varying predictor variable in the risk model. The two longitudinal outcomes are visualized for a random subset of patients in Web Appendix A.2.

3 Interval-censored Cause-specific Joint Models (ICJM) for Longitudinal and Time-to-event Data

To link the repeated measurements of the PSA and core ratio with the time to cancer progression (or treatment initiation), the ICJM jointly models a longitudinal component, in which the underlying development of the biomarkers is captured, and a time-to-event component, in which the risks of the primary and competing events are modeled. Specifically for the Canary PASS data, let T_i^* be the true time of the event that happens first among the $K = 2$ events for the i-th patient. We consider two types of censoring, interval and right censoring. For the interval-censored event, cancer progression ($k = 1$), the true event time is located between the last observed event-free time (i.e., last progression-free biopsy), $T_i^{(1)}$, and the first observed time after the event occurred (i.e., first progression-detected biopsy), T_i. For the observed event, initiation of treatment ($k = 2$), the event-free time, $T_i^{(2)}$, equals the observed time T_i and true event time T_i^* since the event is exactly observed and not interval-censored. When a patient is right-censored, the event-free time for cancer progression is the time of the last observation of the patient's status (i.e., last recorded biopsy, $T_i^{(1)}$), while that for treatment initiation is the censoring time, $T_i^{(2)}$. The vector of event-free times for patient i is thus given by $\boldsymbol{T}_i^{(\mathcal{K})} = \{T_i^{(1)}, T_i^{(2)}\}$.

We denote the repeated observations of the $Q = 2$ longitudinal outcomes, PSA level and core ratio, with $\boldsymbol{y}_{1i}$ and $\boldsymbol{y}_{2i}$ for the i-th patient, respectively. The observed data, denoted by $\boldsymbol{\mathcal{D}}_n = \{\boldsymbol{T}_i^{(\mathcal{K})}, T_i, \boldsymbol{y}_{1i}, \boldsymbol{y}_{2i}; i = 1, \ldots, n\}$ includes information on n subjects.

3.1 Longitudinal Component

To capture the development of the longitudinal outcomes over time, generalized linear mixed models are adopted. Mixed models have the advantage that they allow us to consider multiple longitudinal outcomes

of different types which may be measured at different time points as is the case for the PSA and core ratio.

PSA values are typically right-skewed and previous work has suggested to model the logarithm of PSA + 1 (Pearson et al., 1994; Whittemore et al., 1995). Moreover, preliminary investigations in our own data suggested the assumption of a Student's t-distribution (with three degrees of freedom) for the error terms, $\epsilon_i(t)$. To capture the non-linear evolution of the PSA trajectories, we used a natural cubic spline (with three degrees of freedom) in the fixed and random effects. The model for PSA, hence, had the following structure:

$$\begin{aligned} \log_2(\text{PSA}_i + 1)(t) &= m_{1i}(t) + \epsilon_i(t), \\ m_{1i}(t) &= \beta_0 + b_{0i} + \sum_{p=1}^{3} (\beta_p + b_{pi}) \mathcal{C}_i^{(p)}(t) + \beta_4(\text{Age}_i - 62), \end{aligned} \tag{1}$$

where $\mathcal{C}(t)$ is the design matrix for the natural cubic splines, and Age_i refers to the patient's age at the start of active surveillance, respectively. Baseline age was centered by subtracting the median age (62 years) for computational reasons.

The other repeatedly measured outcome, the core ratio, is the proportion of cores containing cancerous cells. Patients had different numbers of cores sampled (assumed either 12 or 100) at different follow-up times. An exploratory analysis showed a nonlinear trend in the core ratio over time. Compared to the PSA values, nevertheless, the core ratio has fewer measurements. We, thus, specified a binomial mixed model with a quadratic effect over time

$$\begin{aligned} \text{logit}\{\text{E(core ratio)}\} &= m_{2i}(t), \\ m_{2i}(t) &= \beta_5 + b_{4i} + (\beta_6 + b_{5i})t + (\beta_7 + b_{6i})t^2, \end{aligned} \tag{2}$$

where $\text{logit}\{\text{E(core ratio)}\} = \log \frac{\Pr\{\text{core ratio}_i(t)=1\}}{1-\Pr\{\text{core ratio}_i(t)=1\}}$. The random effects from the two longitudinal outcomes, $\boldsymbol{b}_i = (b_{0i}, \ldots, b_{6i})^\top$, are modeled jointly using a multivariate normal distribution with mean zero and variance-covariance matrix $\boldsymbol{D}$. Connecting the two longitudinal outcomes via their random effects allows us to jointly model them despite their different measurement times.

3.2 Time-to-Event Component

The longitudinal component is incorporated in a cause-specific proportional hazard model, which may include additional covariates. The model estimates the hazards of the competing events with separate parameters and baseline hazard functions. The hazard of patient i to experience event k at time t is defined as:

$$\begin{aligned} h_i^{(k)}\left\{t \mid \boldsymbol{\mathcal{M}}_i(t), \boldsymbol{w}_i(t)\right\} &= \lim_{\Delta t \to 0} \frac{\Pr\left\{t \leq T_i^* < t + \Delta t, k \mid T_i^* \geq t, \boldsymbol{\mathcal{M}}_i(t), \boldsymbol{w}_i(t)\right\}}{\Delta t} \\ &= h_0^{(k)}(t) \exp\left[\boldsymbol{\gamma}_k^\top \boldsymbol{w}_i(t) + \sum_{k=1}^{K} \sum_{q=1}^{Q} f_{kq}\{\boldsymbol{m}_{qi}(t), \boldsymbol{\alpha}_{kq}\}\right], \end{aligned}$$

where $\boldsymbol{\mathcal{M}}_i(t) = \{\boldsymbol{m}_{1i}(s), \boldsymbol{m}_{2i}(s); 0 \leq s < t\}$ are the estimated trajectories of the longitudinal outcomes until t, and $\boldsymbol{w}_i(t)$ is a vector of exogenous covariates (in our case, the baseline PSA density), with corresponding regression coefficients $\boldsymbol{\gamma}_k$, $f_{kq}[\cdot]$ denotes the functional form for the effect of the q-th longitudinal outcome, $\boldsymbol{y}_q$, on the hazard of event k, and $\boldsymbol{\alpha}_{kq}$ is the corresponding parameter vector.

For the Canary PASS data, we explored two association structures for the PSA level, the effect of the expected value at time t ($\log_2(\text{PSA} + 1)$ value) and the expected average change between times $t - d$ and t ($\log_2(\text{PSA} + 1)$ velocity), where d is set to one year, i.e.,

$$f_{k1}\left\{\boldsymbol{\mathcal{M}}_{1i}(t), \boldsymbol{\alpha}_{k1}\right\} = \alpha_{1k1} m_{1i}(t) + \alpha_{2k1} \frac{m_{1i}(t) - m_{1i}(t-d)}{d}.$$

For the core ratio, the expected value was considered

$$f_{k2}\left\{\boldsymbol{\mathcal{M}}_{2i}(t), \boldsymbol{\alpha}_{k2}\right\} = \alpha_{1k2} m_{2i}(t).$$

Compared to previous studies where the velocity of a biomarker was represented in the "current slope", mathematically denoted as $m'_{1i}(t) = \frac{dm_{1i}(t)}{dt}$, we opted for the yearly change, because it is more straightforward to interpret from a clinical point of view.

3.3 Estimation

The ICJM can be estimated under the Bayesian framework using Markov chain Monte Carlo (MCMC) methods. The likelihood of the model is derived under the assumption that, conditional on the random effects $\boldsymbol{b}_i$, the survival and longitudinal part are independent, and the repeated measurements of the longitudinal outcomes for the same patient are independent. The likelihood for patient i can be written as:

$$p\left\{\boldsymbol{y}_{1i},\ldots,\boldsymbol{y}_{Qi},\boldsymbol{T}_i^{(\mathcal{K})},T_i,\delta_i \mid \boldsymbol{b}_i,\boldsymbol{\theta}\right\} = \prod_{q=1}^{Q}\prod_{l=1}^{n_{qi}} p(y_{qil} \mid \boldsymbol{b}_{qi},\boldsymbol{\theta}) \times p\left\{\boldsymbol{T}_i^{(\mathcal{K})},T_i,\delta_i \mid \boldsymbol{b}_i,\boldsymbol{\theta}\right\},$$

where δ_i is the indicator of the censoring type with $\delta_i = 0$ for right-censored observations, $\delta_i = 1$ for cancer progression and $\delta_i = 2$ for early treatment initiation. $\boldsymbol{\theta}$ denotes the vector of all model parameters, i.e., $\boldsymbol{\beta}_q$, $\boldsymbol{\gamma}_k$ and $\boldsymbol{\alpha}_{kq}$, for $k = 1, 2$ and $q = 1, 2$. n_{qi} is the number of repeat measurements for longitudinal outcome q for subject i. Taking into account the combination of multiple competing events that may be right- or interval-censored, the likelihood of the time-to-event component for patient i can be written as:

$$\begin{aligned} p(\boldsymbol{T}_i^{(\mathcal{K})},T_i,\delta_i \mid \boldsymbol{b}_i,\boldsymbol{\theta}) = &\left[\exp\left\{-\sum_{k=1}^{K}\int_0^{T_i^{(k)}} h_i^{(k)}(\nu)d\nu\right\}\right]^{I(\delta_i=0)} \\ &\times\left[\int_{T_i^{(1)}}^{T_i} h_i^{(1)}(s)\exp\left\{-\sum_{k=1}^{K}\int_0^{s} h_i^{(k)}(\nu)d\nu\right\}ds\right]^{I(\delta_i=1)} \\ &\times\left[h_i^{(2)}(T_i)\exp\left\{-\sum_{k=1}^{K}\int_0^{T_i^{(k)}} h_i^{(k)}(\nu)d\nu\right\}\right]^{I(\delta_i=2)}. \end{aligned}$$

The first factor (for $\delta_i = 0$), which re-appears in the factor for observed events ($\delta_i = 2$), is the probability of not having experienced any event up until the respective censoring times. Since it is only known that event type k did not happen until the last available observation of the event status, patients contribute to the "overall survival" part of the likelihood only until their event-specific event-free times $T_i^{(k)}$. The integrals in the above equation do not have a closed-form solution, and are numerically approximated using the 15-point Gauss-Kronrod rule. Model estimation using Gibbs sampling combined with the Metropolis–Hastings algorithm can be easily implemented in available software, such as JAGS (Plummer, 2003).

4 Methodology of Personalized Biopsy Schedules

4.1 Personalized Risk of Progression

The ICJM utilizes the full history of relevant biomarker measurements for any patient and models the patient-specific trajectories over time. This enables us to obtain patient-specific and dynamic risk estimates for the main event of interest, cancer progression. Key to this is that the patient-specific information from the longitudinal outcomes is captured in the random effects, which link the longitudinal and survival part of the model. They can, hence, be used to obtain patient-specific risk estimates for a new patient i' based on his history of biomarker values.

Let t_b be the time when the previous biopsy took place, t_m the time of the lastest measurement among the longitudinal outcomes, and t_p the time at which the risk should be predicted. For brevity, the baseline covariates for patient i', $\text{Age}_{i'}$ and $w_{i'}(t)$, are omitted in the following formulas. Using the history of the longitudinal outcomes until t_m, $\boldsymbol{\mathcal{Y}}_{i'}(t_m) = \{\boldsymbol{y}_{1i'}(s_1),\boldsymbol{y}_{2i'}(s_2); 0 \le s_1, s_2 \le t_m\}$, we can formulate the progression-specific cumulative risk at time t_p as

$$\begin{aligned}\Pi^{(1)}_{i'}(t_p \mid t_b, t_m) &= \Pr\{T^*_{i'} \leq t_p, k = 1 \mid T^*_{i'} > t_b, \boldsymbol{\mathcal{Y}}_{i'}(t_m), \boldsymbol{\mathcal{D}}_n\} \\ &= \int\int \Pr(T^*_{i'} \leq t_p, k = 1 \mid T^*_{i'} > t_b, \boldsymbol{b}_{i'}, \boldsymbol{\theta}) p\left\{\boldsymbol{b}_{i'} \mid T^*_{i'} > t_b, \boldsymbol{\mathcal{Y}}_{i'}(t_m), \boldsymbol{\theta}\right\} \\ &\qquad p(\boldsymbol{\theta} \mid \boldsymbol{\mathcal{D}_n}) d\boldsymbol{b}_{i'} d\boldsymbol{\theta},\ t_p > t_b, t_p \geq t_m,\end{aligned}$$

where the second term is the posterior distribution of the random effects $\boldsymbol{b}_{i'}$ conditional on the longitudinal outcomes until time t_m and the patient being event-free until t_b, and the third term is the posterior distribution of the model parameters $\boldsymbol{\theta}$ conditional on the observed data $\boldsymbol{\mathcal{D}}_n$. Of note, we opted for the cumulative incidence function as the event-specific survival does not exist in the competing setting. In the formulation of the progression-specific cumulative risk, the competing risk of early treatment initiation is taken into account by using the joint probability of progression happening before t_p and treatment not being initiated before t_p, denoted here as the joint probability of the event happening before a time t_p and the event being progression.

Inference can be performed using the following Monto Carlo sampling scheme with J iterations (Rizopoulos, 2011): (1) sample $\boldsymbol{\theta}^{(j)}$ from the posterior distribution $p(\boldsymbol{\theta} \mid \boldsymbol{\mathcal{D}_n})$, (2) sample random effects, $\boldsymbol{b}^{(j)}_{i'}$ from their posterior distribution $p\left\{\boldsymbol{b}_{i'} \mid T^*_{i'} > t_b, \boldsymbol{\mathcal{Y}}_{i'}(t_m), \boldsymbol{\theta}^{(j)}\right\}$, (3) calculate the progression-specific risk, $\Pr\left\{T^*_{i'} \leq t_p, k = 1 \mid T^*_{i'} > t_b, \boldsymbol{b}^{(j)}_{i'}, \boldsymbol{\theta}^{(j)}\right\}$, where j is the iteration index. The posterior distribution of the random effects in step (2) is given by

$$p\left\{\boldsymbol{b}_{i'} \mid T^*_{i'} > t_b, \boldsymbol{\mathcal{Y}}_{i'}(t_m), \boldsymbol{\theta}\right\} \propto p(T^*_{i'} > t_b | \boldsymbol{b}_{i'}, \boldsymbol{\theta}) p\left\{\boldsymbol{\mathcal{Y}}_{i'}(t_m) | \boldsymbol{b}_{i'}, \boldsymbol{\theta}\right\} p(\boldsymbol{b}_{i'} | \boldsymbol{\theta}), \tag{3}$$

which does not have a closed form. The Metropolis–Hastings algorithm can be used for sampling the random effects for subject i'. Specifically, we apply the adaptive automatic scaling of the Metropolis–Hastings algorithm using the Robbins-Monro process, as proposed by Garthwaite et al. (2016).

4.2 Generation of Personalized Schedules

To facilitate clinical decision-making, we translate the patient-specific risk estimates into monitoring decisions, i.e., whether a biopsy should be performed at the current clinical visit, and generate a tentative schedule for future biopsies.

This personalized biopsy schedule aims to provide patients with the most suitable biopsy frequencies according to their own risk of cancer progression. In the competing setting, early treatment can interrupt the normal biopsy process and result in fewer biopsies than expected. However, treatment is not random but an active decision. In addition, AS is in place to avoid over-treatment, and starting treatment early is an undesirable behavior in this context. Thus in this study, we focus on utilizing the progression-specific risk derived from the ICJM to generate the personalized biopsy schedules.

Assume $\boldsymbol{T}_p = \{t_p^{(1)}, \ldots, t_p^{(U)}\}$ are the U planned and typically regular clinical visits and eventually result in $N_{i'}$ planned biopsies, $BS^{\phi}_{i'} = \{bs_1, bs_2, ..., bs_{N_{i'}}; bs_{N_{i'}} = t_p^{(U)}\}$. The horizon time until which biopsies should be scheduled is denoted as $t_p^{(U)}$, and $t_p^{(0)} \geq t_m$ is the current visit time. Since the ICJM involves a flexibly modeled baseline hazard function, the distribution of the measurement times in the training data, $\boldsymbol{\mathcal{D}}_n$, should be taken into account when choosing $t_p^{(U)}$ to avoid extrapolation. Setting $t_p^{(U)}$ to a value higher than the, say, 90% percentile of the measurement times in $\boldsymbol{\mathcal{D}}_n$ may lead to overly uncertain and potentially biased predictions. From $t_p^{(1)}$ onward, at each clinical visit $u = 1, \ldots, U$, the current cumulative progression-specific risk is estimated based on the previous (planned) biopsy $bs_{l-1}, l \in \{1, \ldots, N_{i'}\}$ ($u \geq l$ and $bs_0 = t_b$ denotes the time of the last conducted biopsy before scheduling biopsies), and the l^{th} biopsy is scheduled at $bs_l = t_p^{(u)}$ if this estimate exceeds a threshold ϕ, i.e., $\Pi^{(1)}_{i'}(t_p^{(u)} \mid bs_{l-1}, t_m) \geq \phi, \quad \phi \in [0, 1]$. To plan subsequent biopsies, we assume that the just scheduled biopsy does not reveal cancer progression. The estimated risk profile then restarts from zero at the time of that biopsy. The risk estimate for the next clinical visit $u + 1$ is then recalculated conditional on progression happening after the previous (planned) biopsy, $bs_l = t_p^{(u)}$. Otherwise, if the risk estimate at $t_p^{(u)}$ does not exceed ϕ and no biopsy is scheduled at

$t_p^{(u)}$, the risk estimate at $t_p^{(u+1)}$ remains conditional on progression happening after bs_{l-1}. The risk threshold ϕ can either be pre-specified or determined for each patient in a data-driven manner (see Section 4.2.1).

The updating of the time of the previous (planned) biopsy has a consequence for re-sampling the random effects. The posterior distribution of the random effects (Equation 3) is conditional on the time of the previous (planned) biopsy, bs_l, indicating that the random effects for patient i' need to be re-sampled every time a biopsy is (planned to be) scheduled for this patient, leading to a computationally intense procedure. However, this dilemma can be eased by rewriting the risk estimates to the survival (at bs_l)-corrected risk difference between the risks at $t_p^{(u+1)}$ and bs_l

$$\begin{aligned}\Pi_{i'}^{(1)}(t_p^{(u+1)} \mid bs_l, t_m) &= \Pr\{T_{i'}^* \leq t_p^{(u+1)}, k=1 \mid T_{i'}^* > bs_l, T_{i'}^* > t_b, \boldsymbol{\mathcal{Y}}_{i'}(t_m), \boldsymbol{\mathcal{D}}_n\} \\ &= \frac{\Pi_{i'}^{(1)}(t_p^{(u+1)} \mid t_b, t_m) - \Pi_{i'}^{(1)}(bs_l \mid t_b, t_m)}{S(bs_l \mid t_b, t_m)},\end{aligned}$$

where $S(bs_l \mid t_b, t_m)$, the overall survival function at bs_l, has the following formula

$$\begin{aligned}S(bs_l \mid t_b, t_m) &= \Pr\{T_{i'}^* > bs_l \mid T_{i'}^* > t_b, \boldsymbol{\mathcal{Y}}_{i'}(t_m), \boldsymbol{\mathcal{D}}_n\} \\ &= \int\int \Pr(T_{i'}^* > bs_l \mid \boldsymbol{b}_{i'}, \boldsymbol{\theta}) p\left\{\boldsymbol{b}_{i'} \mid T_{i'}^* > t_b, \boldsymbol{\mathcal{Y}}_{i'}(t_m), \boldsymbol{\theta}\right\} p(\boldsymbol{\theta} \mid \boldsymbol{\mathcal{D}_n}) d\boldsymbol{b}_{i'} d\boldsymbol{\theta}.\end{aligned}$$

By conditioning on t_b, instead of bs_l, one whole biopsy schedule can be generated efficiently in the sense that the risk estimates at all future clinical visits can be derived from the risk curve estimated from t_b to $t_p^{(U)}$. As, over time, additional biomarker information is taken, the posterior distribution of the random effects depending on $\boldsymbol{\mathcal{Y}}_{i'}(t_m)$ (where t_m is now the time of the new biomarker measurements) needs adjustment, and risk estimates should be derived from the updated one. Consequently, the proposed biopsy schedule is correspondingly updated and the data-driven risk threshold may also be altered.

We base the decision to schedule a biopsy on the risk of progression but not on the risk of the competing event, since biopsies are not needed to determine the occurrence of the competing event of early treatment initiation. In other applications, however, the occurrence of multiple competing events may be determined by the same diagnostic test. In that case, the cumulative risk for any of these events should be considered when determining whether the test should be performed or deferred.

4.2.1 Choice of the Risk Threshold

The choice of risk threshold influences the resulting biopsy schedule. A higher risk threshold results in a higher risk of missing the optimal treatment window. Since patients progress at different rates, different risk thresholds may be appropriate. We follow the idea of Tomer et al. (2022) to choose a suitable patient-specific risk threshold by balancing the expected number of biopsies and expected delay in detection (see Figure 1) and adapt their proposed methodology to the setting with competing risks.

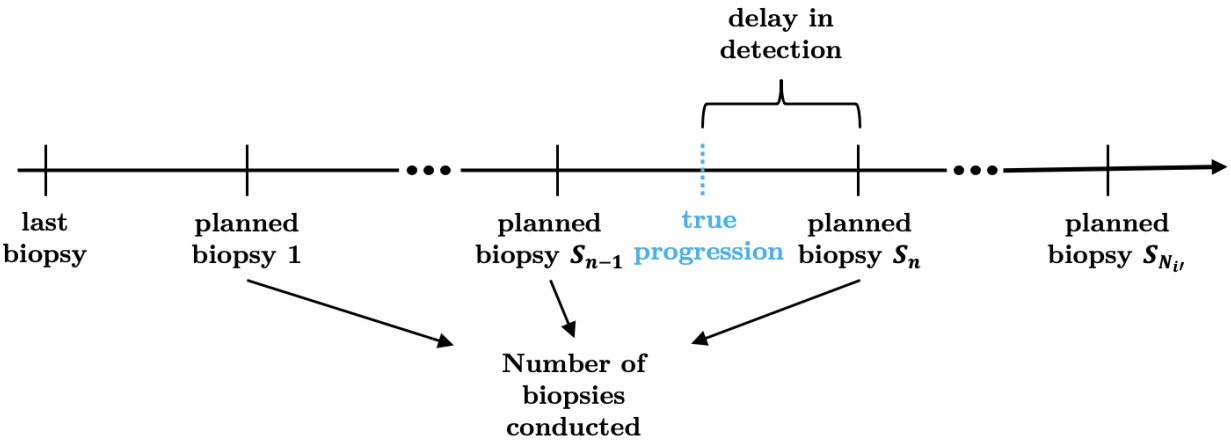

Figure 1: Definition for the number of biopsies (Nb) and detection delay (Dd).

Given a proposed biopsy schedule $BS_{i'}^{\phi}$, the time for the last conducted biopsy before the personalized schedule bs_0, and a horizon time $t_p^{(U)}$, the number of biopsies (Nb) for patients who experience progression or start early treatment is

$$\begin{aligned} Nb(BS_{i'}^{\phi}) = l, \quad &\text{if } bs_{l-1} < T_{i'}^* \leq bs_l, k = 1, \text{ or} \\ Nb(BS_{i'}^{\phi}) = l-1, \quad &\text{if } bs_{l-1} < T_{i'}^* \leq bs_l, k = 2. \end{aligned}$$

Patients who do not experience either event before $t_p^{(U)}$ undergo all $N_{i'}$ scheduled biopsies. The detection delay (Dd) is expressed as

$$Dd(BS_{i'}^{\phi}) = bs_l - T_{i'}^*, \quad \text{if } bs_{l-1} < T_{i'}^* \leq bs_l, k = 1,$$

with $l \in \{1, \ldots, N_{i'}\}$. For patients who are event-free or start early treatment, the detection delay is undefined as cancer progression does not occur. Since our interest is in the detection of progression and early treatment is not the focus in evaluating a biopsy schedule, this is not regarded as a restriction in our setting.

Since the actual number of biopsies to be conducted is unknown when creating a schedule and the true progression time is generally unknown in practice, we use the expected number of biopsies and expected delay in detection instead. The expected number of biopsies is:

$$E\{Nb(BS_{i'}^{\phi})\} = \sum_{l=1}^{N_{i'}} l \times \Pr\{bs_{l-1} < T_{i'}^* \leq bs_l \mid T_{i'}^* \leq bs_{N_{i'}}, k = 1\},$$

where

$$\Pr\{bs_{n-1} < T_{i'}^* \leq bs_n \mid T_{i'}^* \leq bs_{N_{i'}}, k = 1\} = \frac{\Pi_{i'}^{(1)}(bs_n \mid t_b, t_m) - \Pi_{i'}^{(1)}(bs_{n-1} \mid t_b, t_m)}{\Pi_{i'}^{(1)}(bs_{N_{i'}} \mid t_b, t_m)},$$

and the expected detection delay can be calculated as:

$$E\{Dd(BS_{i'}^{\phi})\} = \sum_{l=1}^{N_{i'}} \Big[\{bs_l - E(T_{i'}^* \mid bs_{l-1}, bs_l, t_m, k = 1)\} \times \Pr\{bs_{l-1} < T_{i'}^* \leq bs_l \mid T_{i'}^* < bs_{N_{i'}}, k = 1\} \Big],$$

where the expected progression time for subject i' between two biopsies bs_{l-1} and bs_l is

$$\begin{aligned} E(T_{i'}^* \mid bs_{l-1}, bs_l, t_m, k = 1) &= bs_{l-1} + \int_{bs_{l-1}}^{bs_l} \Pr\{T_{i'}^* \geq v \mid bs_{l-1} < T_{i'}^* \leq bs_l, k = 1, \boldsymbol{\mathcal{Y}}_{i'}(t_m), \boldsymbol{D}_n\} dv \\ &= bs_{l-1} + \int_{bs_{l-1}}^{bs_l} \frac{\Pr\{v \leq T_{i'}^* \leq bs_l \mid k = 1, \boldsymbol{\mathcal{Y}}_{i'}(t_m), \boldsymbol{D}_n\}}{\Pr\{bs_{l-1} < T_{i'}^* \leq bs_l \mid k = 1, \boldsymbol{\mathcal{Y}}_{i'}(t_m), \boldsymbol{D}_n\}} dv. \end{aligned}$$

For determining the patient-specific risk threshold, we utilize a grid search, creating schedules with a range of thresholds, each with its own expected number of biopsies and delay. Which of the resulting schedules is optimal depends on how the number of biopsies are weighted against the delay. Using weights (w_1 and w_2) we can then define the optimal schedule as the one that minimizes the Euclidean distance of the expected number of biopsies and delay. This is visualized in Figure 2 and can be determined as

$$\phi_{i'}^*(v) = \underset{\phi_{i'} \in [0,1]}{\operatorname{argmin}} \sqrt{w_1 \times \Big[E\{Nb(BS_{i'}^{\phi})\} - 1\Big]^2 + w_2 \times \Big[E\{Dd(BS_{i'}^{\phi})\} - 0\Big]^2}.$$

For simplicity, we fix the weights w_1 and w_2 to one. In practice, ensuring the detection delay does not exceed a particular value may be desirable. This can be added as a constraint to the optimization. As over time, new biomarker measurements are collected, the optimization process is repeated dynamically to provide personal schedules that take into account all available information.

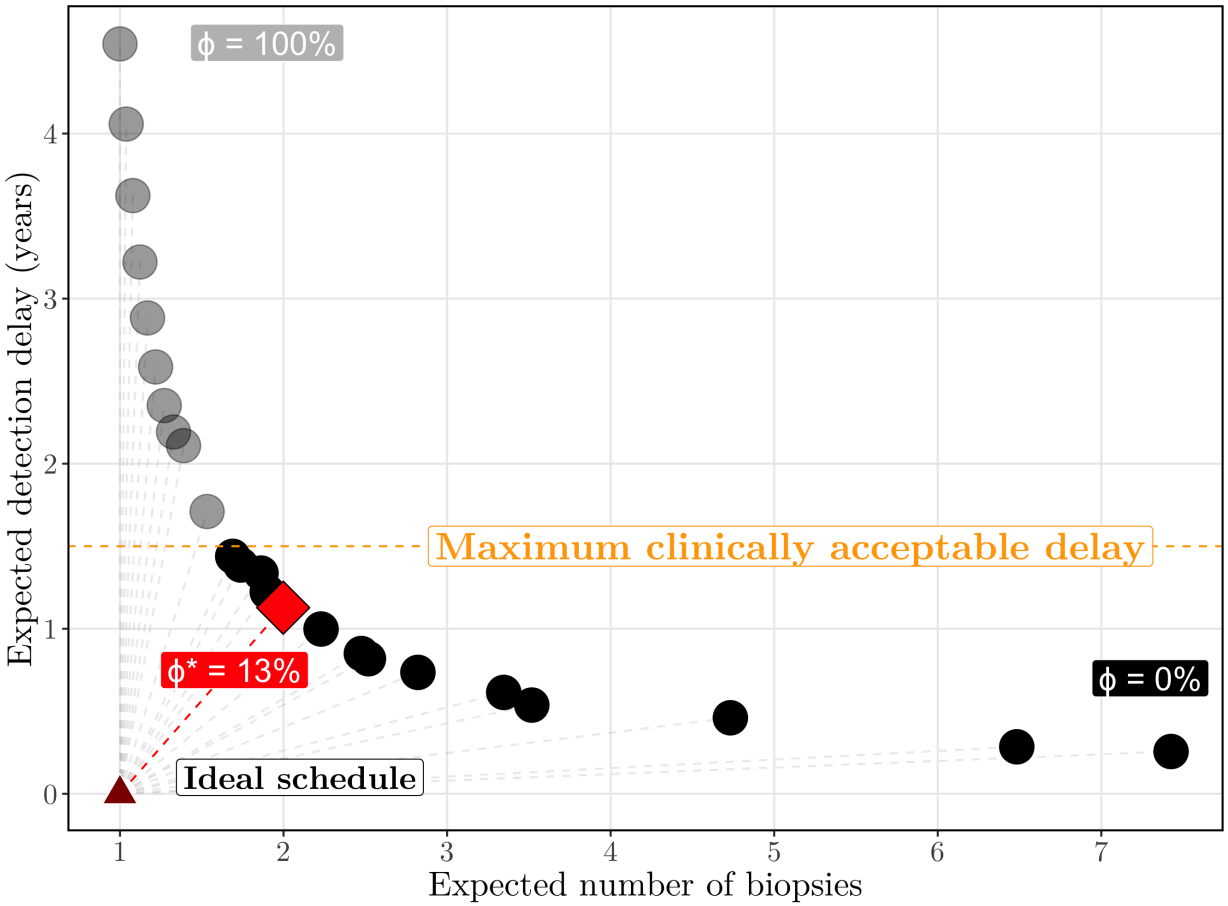

Figure 2: Choice of the optimal risk threshold based on the expected number of biopsies and detection delay.

5 Analysis of the Canary PASS Data

We analyzed the Canary PASS data using two ICJMs. The primary model (ICJM 1) is based on the PSA as the main predictor of cancer progression. PSA trajectories were modeled with a Student's-t mixed model, indicated in Equation (1). Besides, the estimated (underlying) value of PSA at the time of an event, the time-to-event component included the change in the estimated PSA over the previous year, and the patient's age and PSA density at baseline.

To explore the role of the core ratio, we extended ICJM 1 with a binomial mixed model for the core ratio, indicated in Equation (2), and included the estimated value of this ratio in the time-to-event component (ICJM 2).

The most relevant parameter estimates from both models are summarized in Table 1. For the full result table, see Web Appendix D.3. The results from the survival component of primary model reveal that with a one unit increase in log(baseline PSA density), the estimated risk of progression increased by a factor 1.66 (95% credible interval, CI: 1.27-2.14). Moreover, an increase of the $\log_2(\text{PSA}+1)$ by one increased the progression-specific risk by a factor of 1.14 (95% CI: 0.92-1.41) while increasing the change in $\log_2(\text{PSA}+1)$ over the previous year by one led to a 23.26 (95% CI: 5.24-65.25)-fold increase in the risk. In ICJM2, the hazard ratio (HR) for log(baseline PSA density) was reduced to 1.40 (95% CI: 1.02-1.86) while the impact of the $\log_2(\text{PSA}+1)$ value was amplified (HR increased to 1.27, 95% CI: 0.98-1.60) and that from its yearly change was weakened (HR decreased to 8.40, 95% CI: 1.75-23.91). Besides, a one-unit increase in the logit[E(core ratio)] led to a 2.20 (95% CI: 1.61-2.90)-fold increment in the progression-specific risk.

Notably, the $\log_2(\text{PSA}+1)$ and logit[E(core ratio)] also played important roles in the risk of initiating

Table 1: Estimated parameters in the joint model for the Canary PASS data.

Parameters	**ICJM 1 (PSA)**		**ICJM 2 (PSA & core ratio)**	
	HR	**95% CI**	**HR**	**95% CI**
Progression-specific survival component				
log(PSA density)	1.66	[1.27, 2.14]	1.40	[1.02, 1.86]
$\log_2(\text{PSA}+1)$ value	1.14	[0.92, 1.41]	1.27	[0.98, 1.60]
$\log_2(\text{PSA}+1)$ yearly change	24.26	[6.24, 66.25]	8.40	[1.75, 23.91]
logit[E(core ratio)] value	-	-	3.20	[2.61, 3.90]
Treatment-specific survival component				
log(PSA density)	1.29	[0.82, 1.93]	0.73	[0.39, 1.25]
$\log_2(\text{PSA}+1)$ value	1.54	[1.11, 2.09]	1.93	[1.22, 3.01]
$\log_2(\text{PSA}+1)$ yearly change	23.47	[1.86, 108.49]	19.24	[0.58, 107.31]
logit[E(core ratio)] value	-	-	6.50	[4.24, 10.23]

CI: credible interval; HR: hazard ratio; Note: the longitudinal components are not shown.

early treatment. Increasing the $\log_2(\text{PSA}+1)$ and logit[E(core ratio)] by one unit resulted in an increased risk of early treatment by a factor of 1.93 (95% CI: 1.22-3.01) and 6.50 (95% CI: 4.24-10.23), respectively. This indicates that if a patient has a higher PSA level or a larger core ratio in a biopsy, he does not only have a higher probability of cancer progression, but is also more likely to start early treatment.

To facilitate the interpretation of the results in light of the transformed scale, we present effect plots in the original scale (Figure 3 and Figure 4). In the effect plots, the mean PSA level of 5 ng/ml and the mean PSA yearly change of 0.3 ng/ml for patients with median age of 62 were taken as a reference. Figure 3(a) shows that doubling the PSA level (to 10 ng/ml) resulted in a hazard ratio for cancer progression of 1.23 (95% CI: 1.00-1.51), while halving the PSA level resulted in a 17% (95% CI: 0%-31%) decrease of the risk, assuming other covariates remaining constant. As shown in Figure 3(b), doubling the PSA yearly change (to 0.6 ng/ml) led to a 0.16 (95% CI: 0.04-0.28)-fold increase of the risk of progression, while halving the PSA yearly change resulted in a 7% (95% CI: 2%-11%) decrease of the risk.

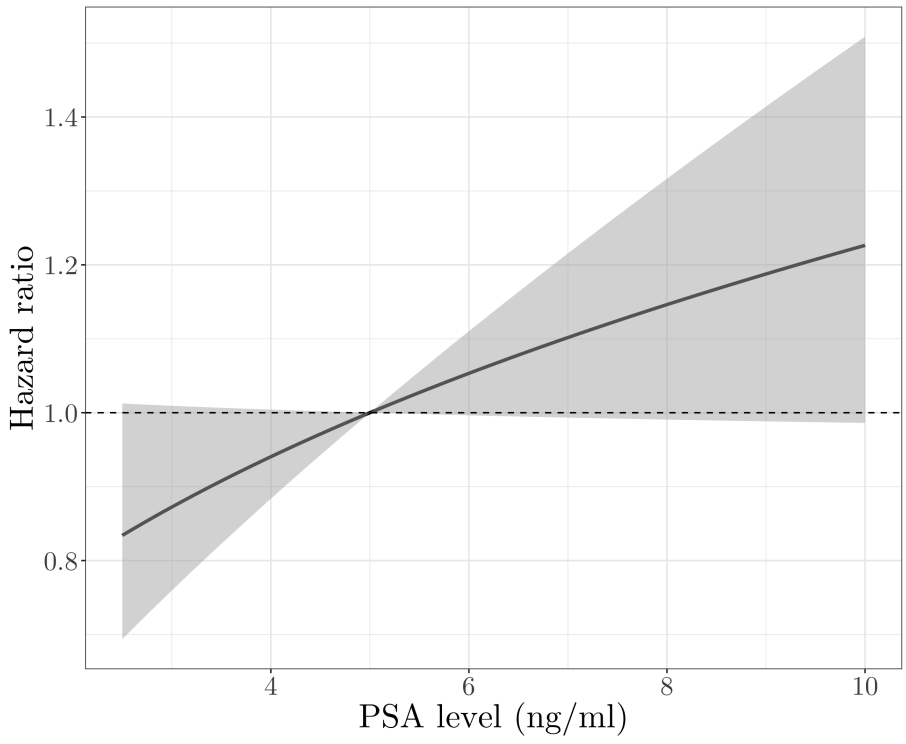

(a)

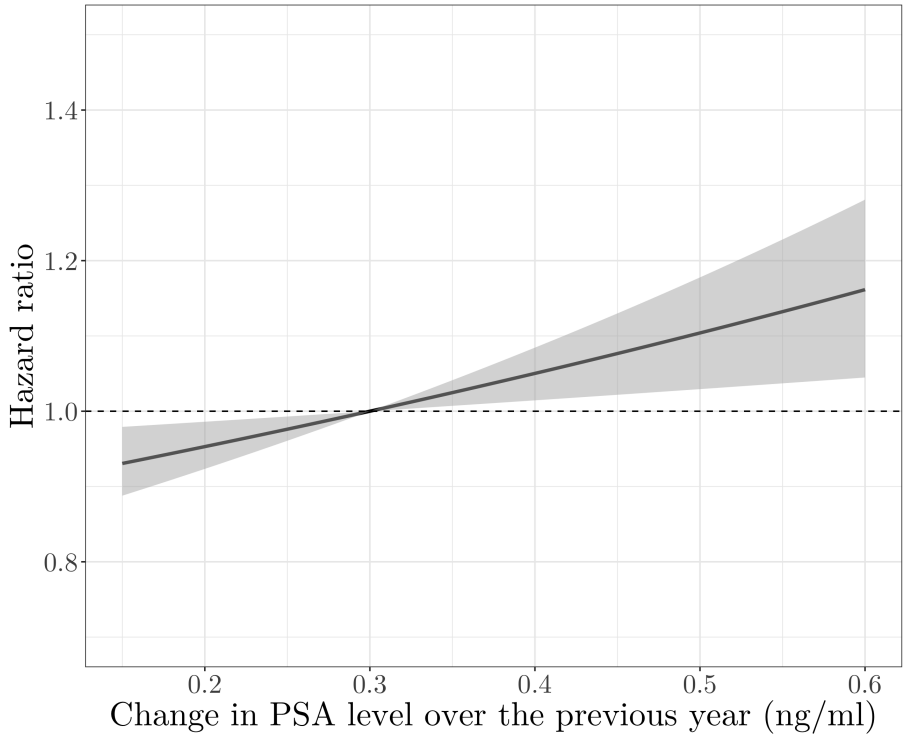

(b)

Figure 3: Effect plot for the impact of (a) the value of PSA and (b) the change in PSA over the previous year on the estimated risk of progression with reference to (a) PSA value 5 ng/ml and (b) change of 0.3 ng/ml, other covariates remaining constant.

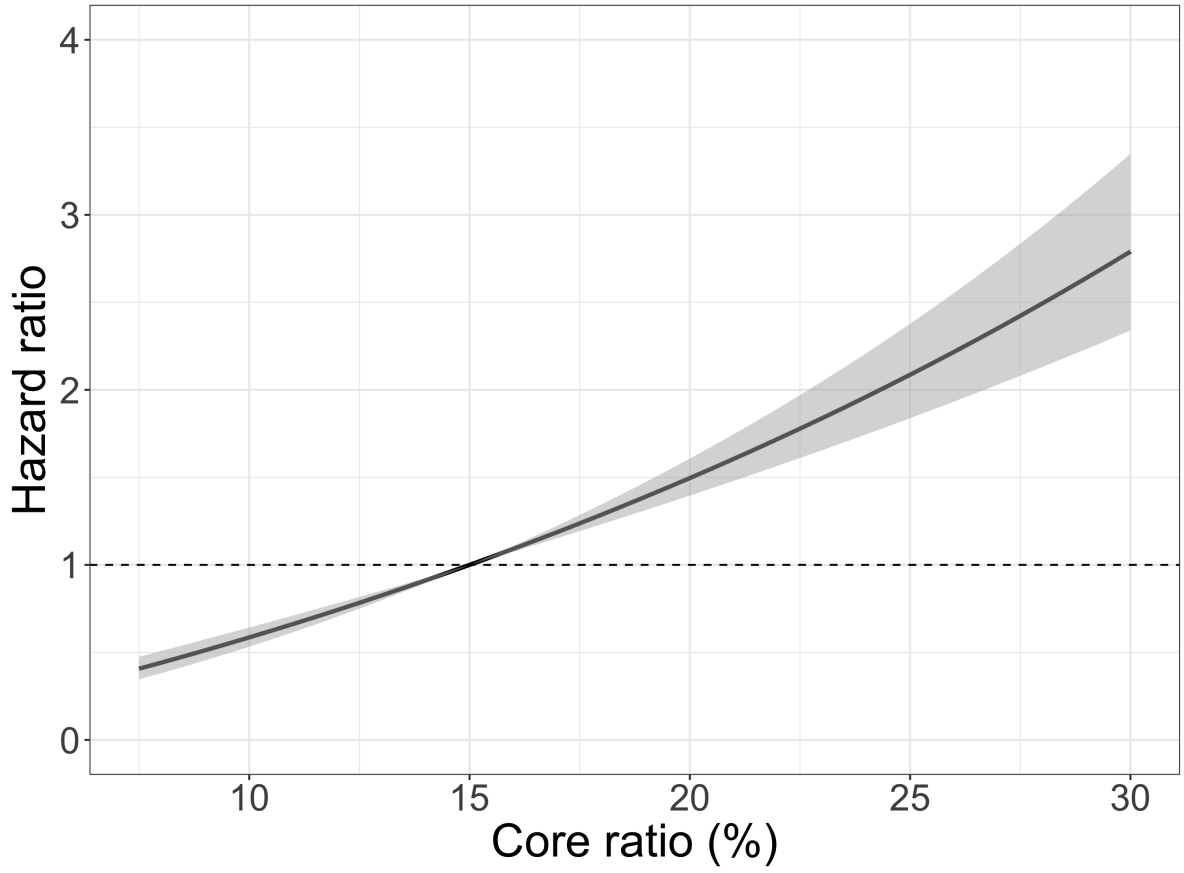

Figure 4: Effect of the core ratio value (contrast to a core ratio of 15%) on the risk of progression, other covariates remaining constant.

The estimated effect of the core ratio is visualized in Figure 4. The observed average core ratio of 15% was taken as reference. Doubling the core ratio to 30% raised the progression-specific risk by a factor of 2.79 (95% CI: 2.34-3.35) while halving the core ratio lowered the risk by 59% (95% CI: 53%-65%).

The efficacy of the personalized biopsy schedules cannot be directly evaluated on the observed data since a fixed schedule following the PASS protocol has been implemented there. Therefore, a simulation study is launched in the following section for implementing personalized biopsy schedules.

6 Simulation

We conducted a simulation study to evaluate the efficiency of the proposed personalized biopsy schedules and compare it with that of two existing fixed schedules. The different schedules are evaluated based on the indicators introduced above, the number of biopsies the patients undergo from entering AS and the delay between cancer progression and detection of progression. Since, in this simulation, the progression time is known, the actual delay and number of conducted biopsies are used in the evaluation and comparison (while the expected values are used for generating the schedules). In Section 6.1, the simulation procedures and scenarios are presented. The results are summarized in Section 6.2.

6.1 Simulation Setting

Data were simulated based on the primary ICJM fitted on the Canary PASS data (ICJM 1 in Section 5). In total, 200 datasets were created, each of which was split into a training set of 300 subjects and a test set of 200 subjects. Each test set contained 100 subjects with progression and 100 subjects without progression.

We compared the personalized schedules with a fixed schedule of yearly biopsies and the schedule from the Canary PASS protocol (see Section 2). Since the personalized schedules rely on predictions of the progression-specific risk, we also evaluated the predictive performance of the ICJM, see Web Appendix C.2.

For each simulated dataset, we fitted the ICJM on the training set and generated personalized schedules for the subjects in the test set. All subjects in the test set were assumed to have an initial (progression-negative) biopsy when entering AS (i.e., at time zero), visit the clinics every six months, and have PSA levels evaluated every three months. Schedules were generated for a horizon time of 10 years. The maximum acceptable expected delay for the personalized schedules was fixed to 1.5 years.

6.2 Simulation Results

The simulation results are visualized in Figure 5. For patients whose cancer progression had been detected, the median number of biopsies (including the initial biopsy) was four in the PASS schedule and five in the annual schedule, but the personalized biopsy schedules required only a median of two biopsies, resulting in an average decrease of 1.52 (34%) and 2.57 (42%) biopsies per patient compared to the PASS and annual fixed schedule, respectively. As a trade-off, the personalized schedules resulted in a moderately longer detection delay of 1.40 years (median) compared to 0.93 years delay for the PASS schedule and 0.50 years delay for the annual biopsies. For patients who did not experience cancer progression before the horizon time, we observe that the personalized schedules reduced the number of biopsies by on average, 1.60 (46%) and 2.66 (54%) per patient compared to the PASS biopsy schedule and the annual biopsy schedule, respectively.

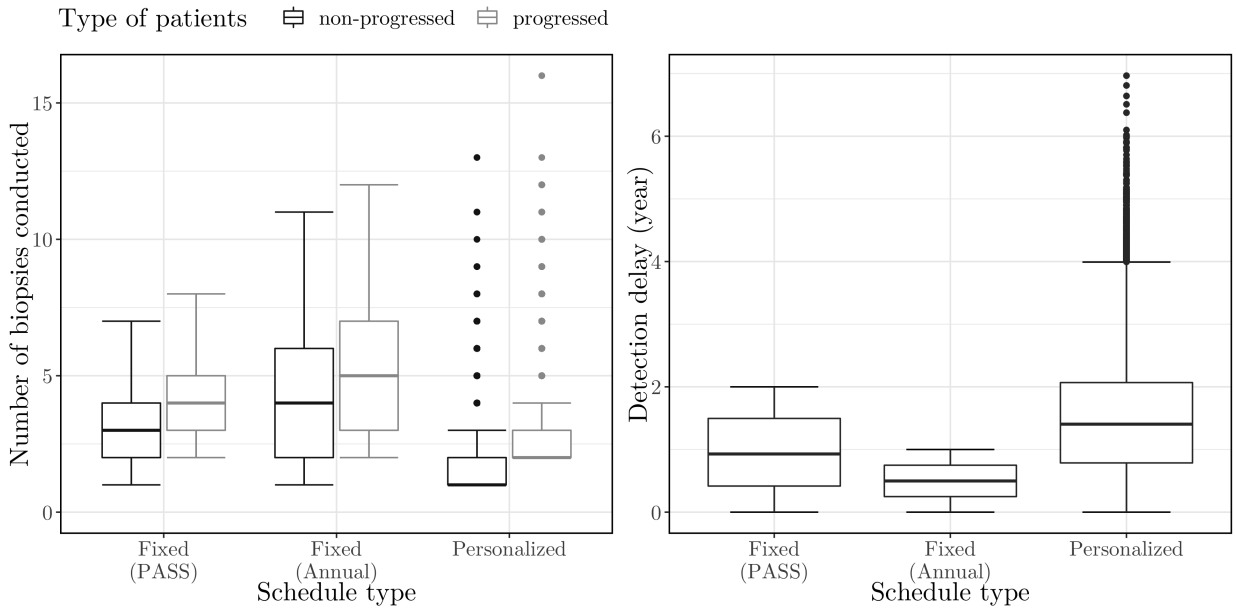

Figure 5: Number of biopsies (including the biopsy conducted when entering the AS) for all 200 × 200 patients and detection delay for 200 × 100 progressed patients in the test sets .

7 Discussion

In this study, we proposed the interval-censored cause-specific joint model to estimate the patient-specific risk of cancer progression in AS of prostate cancer patients, using longitudinal biomarkers while considering the competing risk of early treatment initiation. These risk profiles were then used to generate personalized biopsy schedules. In our simulation study, the personalized schedules reduced the number of biopsies per patient on average by 34%-54% compared to two fixed schedules. As a trade-off, the personalized schedules lead to slightly longer detection delays.

Our proposed methodology extends the work of Tomer et al. (2022). The ICJM retains the qualities of the standard joint model to handle endogeneity and random measurement error in the longitudinal outcomes but also takes into account the interval censoring of cancer progression and the informative censoring due to early treatment initiation. Especially considering the competing event aids the ICJM in reducing bias in predicting risk of cancer progression necessary for informed decision-making. The simulation study showing the efficacy of the methodology for personalized biopsy schedules focused on the PSA as the main predictor of cancer progression. The ICJM can be easily extended with additional longitudinal outcomes and handle the issue of different timelines in different longitudinal biomarkers, as demonstrated in ICJM 2 with the core ratio. Considering more longitudinal outcomes may further improve the predictive ability of the ICJM and thus the quality of the personalized schedules. With the increase in the dimensionality of the ICJM, shrinkage methods may become relevant (Andrinopoulou and Rizopoulos, 2016).

The frequency and timing of biopsies in our personalized schedules are based on a trade-off between the resulting expected number of biopsies and expected delay in detecting progression. Since these two indicators are on very different scales, it is not clear how they should be weighted relative to each other. More information on how detection delay is related to clinical outcomes, such as mortality, is needed to better tailor this trade-off to the actual risks associated with a particular schedule. It may also be worth exploring whether this relationship differs by patient characteristics like the patient's age or time since the start of active surveillance. Studies with longer follow-up, for instance, where patients are monitored until death, or microsimulation models (De Carvalho et al., 2017), may help to gain the necessary insights.

Further adaptations of the methodology are necessary to reflect the actual clinical setting more closely. For example, the current approach does not yet consider that biopsies are imperfect measurements and may give false-negative results. Moreover, other diagnostic tools, such as magnetic resonance imaging (MRI), are utilized in clinical practice to guide the decision to perform a biopsy. Future extensions might, thus, consider the additional uncertainty due to false-negative biopsies and more complex decision-making processes.

In conclusion, the proposed ICJM allows us to obtain patient-specific dynamic risk predictions for interval-censored events in the presence of competing risks that can be translated to personalized biopsy schedules for prostate cancer patients in AS. The resulting schedules can relieve the burden on patients by considerably reducing the number of biopsies while limiting the delay in detecting cancer progression.

Acknowledgements

The research was funded by the National Institutes of Health (the NIH CISNET Prostate Award CA253910). The authors would also like to show our gratitude to the Canary PASS team and all study participants.

References

Adamy, A., Yee, D. S., Matsushita, K., Maschino, A., Cronin, A., Vickers, A., Guillonneau, B., Scardino, P. T., and Eastham, J. A. (2011). Role of prostate specific antigen and immediate confirmatory biopsy in predicting progression during active surveillance for low risk prostate cancer. *The Journal of Urology* **185,** 477–482.

Aizer, A. A., Gu, X., Chen, M.-H., Choueiri, T. K., Martin, N. E., Efstathiou, J. A., Hyatt, A. S., Graham, P. L., Trinh, Q.-D., Hu, J. C., and Nguyen, P. L. (2015). Cost implications and complications of overtreatment of low-risk prostate cancer in the United States. *Journal of the National Comprehensive Cancer Network* **13,** 61–68.

Albertsen, P. C., Hanley, J. A., and Fine, J. (2005). 20-year outcomes following conservative management of clinically localized prostate cancer. *JAMA* **293,** 2095–2101.

Andrinopoulou, E.-R. and Rizopoulos, D. (2016). Bayesian shrinkage approach for a joint model of longitudinal and survival outcomes assuming different association structures. *Statistics in Medicine* **35,** 4813–4823.

Bruinsma, S. M., Bokhorst, L. P., Roobol, M. J., and Bangma, C. H. (2016). How often is biopsy necessary in patients with prostate cancer on active surveillance? *Journal of Urology* **195,** 11–12.

Bul, M., Zhu, X., Valdagni, R., Pickles, T., Kakehi, Y., Rannikko, A., Bjartell, A., Van Der Schoot, D. K., Cornel, E. B., Conti, G. N., Boevé, E. R., Staerman, F., Vis-Maters, J. J., Vergunst, H., Jaspars, J. J., Strölin, P., Van Muilekom, E., Schröder, F. H., Bangma, C. H., and Roobol, M. J. (2013). Active surveillance for low-risk prostate cancer worldwide: the PRIAS study. *European Urology* **63,** 597–603.

Cary, K. C. and Cooperberg, M. R. (2013). Biomarkers in prostate cancer surveillance and screening: past, present, and future. *Therapeutic Advances in Urology* **5,** 318–329.

Chen, R. C., Rumble, R. B., Loblaw, D. A., Finelli, A., Ehdaie, B., Cooperberg, M. R., Morgan, S. C., Tyldesley, S., Haluschak, J. J., Tan, W., Justman, S., and Jain, S. (2016). Active surveillance for the management of localized prostate cancer (Cancer Care Ontario Guideline): American Society of Clinical Oncology clinical practice guideline endorsement. *Journal of Clinical Oncology: Official Journal of the American Society of Clinical Oncology* **34,** 2182–2190.

Cooperberg, M. R., Zheng, Y., Faino, A. V., Newcomb, L. F., Zhu, K., Cowan, J. E., Brooks, J. D., Dash, A., Gleave, M. E., Martin, F., Morgan, T. M., Nelson, P. S., Thompson, I. M., Wagner, A. A., Carroll, P. R., and Lin, D. W. (2020). Tailoring intensity of active surveillance for low-risk prostate cancer based on individualized prediction of risk stability. *JAMA Oncology* **6,** e203187–e203187.

Dall'Era, M. A., Cooperberg, M. R., Chan, J. M., Davies, B. J., Albertsen, P. C., Klotz, L. H., Warlick, C. A., Holmberg, L., Bailey Jr, D. E., Wallace, M. E., Kantoff, P. W., and Carroll, P. R. (2008). Active surveillance for early-stage prostate cancer. *Cancer* **112,** 1650–1659.

Davis, J. W., Ward, J. F. r., Pettaway, C. A., Wang, X., Kuban, D., Frank, S. J., Lee, A. K., Pisters, L. L., Matin, S. F., Shah, J. B., Karam, J. A., Chapin, B. F., Papadopoulos, J. N., Achim, M., Hoffman, K. E., Pugh, T. J., Choi, S., Troncoso, P., Logothetis, C. J., and Kim, J. (2016). Disease reclassification risk with stringent criteria and frequent monitoring in men with favourable-risk prostate cancer undergoing active surveillance. *BJU International* **118,** 68–76.

De Carvalho, T. M., Heijnsdijk, E. A., and De Koning, H. J. (2017). Estimating the risks and benefits of active surveillance protocols for prostate cancer: a microsimulation study. *BJU International* **119,** 560–566.

Eminaga, O., Shkolyar, E., Breil, B., Semjonow, A., Boegemann, M., Xing, L., Tinay, I., and Liao, J. C. (2022). Artificial intelligence-based prognostic model for urologic cancers: a SEER-based study. *Cancers* **14,**.

Gandaglia, G., Leni, R., Bray, F., Fleshner, N., Freedland, S. J., Kibel, A., Stattin, P., Van Poppel, H., and La Vecchia, C. (2021). Epidemiology and prevention of prostate cancer. *European Urology Oncology* **4,** 877–892.

Garthwaite, P. H., Fan, Y., and Sisson, S. A. (2016). Adaptive optimal scaling of Metropolis–Hastings algorithms using the Robbins–Monro process. *Communications in Statistics - Theory and Methods* **45,** 5098–5111.

Godtman, R. A., Holmberg, E., Khatami, A., Pihl, C.-G., Stranne, J., and Hugosson, J. (2016). Long-term results of active surveillance in the Göteborg randomized, population-based prostate cancer screening trial. *European Urology* **70,** 760–766.

Ishwaran, H., Kogalur, U. B., Blackstone, E. H., and Lauer, M. S. (2008). Random survival forests. *The Annals of Applied Statistics* **2,** 841 – 860.

Klotz, L., Vesprini, D., Sethukavalan, P., Jethava, V., Zhang, L., Jain, S., Yamamoto, T., Mamedov, A., and Loblaw, A. (2015). Long-term follow-up of a large active surveillance cohort of patients with prostate cancer. *Journal of Clinical Oncology : Official Journal of the American Society of Clinical Oncology* **33,** 272–277.

Lee, C., Light, A., Saveliev, E. S., Van der Schaar, M., and Gnanapragasam, V. J. (2022). Developing machine learning algorithms for dynamic estimation of progression during active surveillance for prostate cancer. *npj Digital Medicine* **5,** 110.

Lowenstein, L. M., Basourakos, S. P., Williams, M. D., Troncoso, P., Gregg, J. R., Thompson, T. C., and Kim, J. (2019). Active surveillance for prostate and thyroid cancers: evolution in clinical paradigms and lessons learned. *Nature Reviews. Clinical Oncology* **16,** 168–184.

Mamawala, M. M., Rao, K., Landis, P., Epstein, J. I., Trock, B. J., Tosoian, J. J., Pienta, K. J., and Carter, H. B. (2017). Risk prediction tool for grade re-classification in men with favourable-risk prostate cancer on active surveillance. *BJU International* **120,** 25–31.

Nayan, M., Salari, K., Bozzo, A., Ganglberger, W., Lu, G., Carvalho, F., Gusev, A., Schneider, A., Westover, B. M., and Feldman, A. S. (2022). A machine learning approach to predict progression on active surveillance for prostate cancer. *Urologic Oncology: Seminars and Original Investigations* **40,** 161.e1–161.e7.

Nelson, T. J., Javier-DesLoges, J., Deka, R., Courtney, P. T., Nalawade, V., Mell, L., Murphy, J., Parsons, J. K., and Rose, B. S. (2021). Association of prostate-specific antigen velocity with clinical progression among African American and non-Hispanic white men treated for low-risk prostate cancer with active surveillance. *JAMA Network Open* **4,** e219452–e219452.

Newcomb, L. F., Thompson, I. M. J., Boyer, H. D., Brooks, J. D., Carroll, P. R., Cooperberg, M. R., Dash, A., Ellis, W. J., Fazli, L., Feng, Z., Gleave, M. E., Kunju, P., Lance, R. S., McKenney, J. K., Meng, M. V., Nicolas, M. M., Sanda, M. G., Simko, J., So, A., Tretiakova, M. S., Troyer, D. A., True, L. D., Vakar-Lopez, F., Virgin, J., Wagner, A. A., Wei, J. T., Zheng, Y., Nelson, P. S., and Lin, D. W. (2016). Outcomes of active surveillance for clinically localized prostate cancer in the prospective, multi-institutional Canary PASS cohort. *The Journal of Urology* **195,** 313–320.

Pearson, J. D., Morrell, C. H., Landis, P. K., Carter, H. B., and Brant, L. J. (1994). Mixed-effects regression models for studying the natural history of prostate disease. *Statistics in Medicine* **13,** 587–601.

Pernar, C. H., Ebot, E. M., Wilson, K. M., and Mucci, L. A. (2018). The epidemiology of prostate cancer. *Cold Spring Harbor Perspectives in Medicine* **8,** a030361.

Plummer, M. (2003). JAGS: a program for analysis of bayesian graphical models using Gibbs sampling. In Hornik, K., Leisch, F., and Zeileis, A., editors, *Proceedings of the 3rd International Workshop on Distributed Statistical Computing (DSC 2003)*. ISSN: 1609-395X.

Rizopoulos, D. (2011). Dynamic predictions and prospective accuracy in joint models for longitudinal and time-to-event data. *Biometrics* **67,** 819–829.

Schuster, N. A., Hoogendijk, E. O., Kok, A. A., Twisk, J. W., and Heymans, M. W. (2020). Ignoring competing events in the analysis of survival data may lead to biased results: a nonmathematical illustration of competing risk analysis. *Journal of Clinical Epidemiology* **122,** 42–48.

Selvadurai, E. D., Singhera, M., Thomas, K., Mohammed, K., Woode-Amissah, R., Horwich, A., Huddart, R. A., Dearnaley, D. P., and Parker, C. C. (2013). Medium-term outcomes of active surveillance for localised prostate cancer. *European Urology* **64,** 981–987.

Tomer, A., Nieboer, D., Roobol, M. J., Steyerberg, E. W., and Rizopoulos, D. (2019). Personalized schedules for surveillance of low-risk prostate cancer patients. *Biometrics* **75,** 153–162.

Tomer, A., Nieboer, D., Roobol, M. J., Steyerberg, E. W., and Rizopoulos, D. (2022). Shared decision making of burdensome surveillance tests using personalized schedules and their burden and benefit. *Statistics in Medicine* **41,** 2115–2131.

Tosoian, J. J., Trock, B. J., Landis, P., Feng, Z., Epstein, J. I., Partin, A. W., Walsh, P. C., and Carter, H. B. (2011). Active surveillance program for prostate cancer: an update of the Johns Hopkins experience. *Journal of Clinical Oncology: Official Journal of the American Society of Clinical Oncology* **29,** 2185–2190.

Welty, C. J., Cowan, J. E., Nguyen, H., Shinohara, K., Perez, N., Greene, K. L., Chan, J. M., Meng, M. V., Simko, J. P., Cooperberg, M. R., and Carroll, P. R. (2015). Extended followup and risk factors for disease reclassification in a large active surveillance cohort for localized prostate cancer. *The Journal of Urology* **193,** 807–811.

Whittemore, A. S., Wu, A. H., Kolonel, L. N., John, E. M., Gallagher, R. P., Howe, G. R., West, D. W., Teh, C.-Z., and Stamey, T. (1995). Family history and prostate cancer risk in black, white, and asian men in the United States and Canada. *American Journal of Epidemiology* **141,** 732–740.

Zhou, G.-Q., Wu, C.-F., Deng, B., Gao, T.-S., Lv, J.-W., Lin, L., Chen, F.-p., Kou, J., Zhang, Z.-X., Huang, X.-D., Zheng, Z.-Q., Ma, J., Liang, J.-H., and Sun, Y. (2020). An optimal posttreatment surveillance strategy for cancer survivors based on an individualized risk-based approach. *Nature Communications* **11,** 3872.

Supporting information - Personalized Biopsy Schedules Using an Interval-censored Cause-specific Joint Model

Zhenwei Yang[1,2], Dimitris Rizopoulos[1,2], Eveline A.M. Heijnsdijk[3], Lisa F. Newcomb[4], and Nicole S. Erler[1,2]

[1]Department of Biostatistics, Erasmus Medical Center Rotterdam
[2]Department of Epidemiology, Erasmus Medical Center Rotterdam
[3]Department of Public Health, Erasmus Medical Center Rotterdam
[4]Fred Hutchinson Cancer Research Center, Cancer Prevention Program, Public Health Sciences, Seattle, Washington

January 3, 2023

Web Appendix A Data

Web Appendix A.1 PASS Data

Web Table 1 summarizes the relevant subset of the Canary PASS data.

Web Table 1: Summary table for the Canary PASS Data.

Item	**Value**
Number of subjects	833
Observation time until progression/treatment (years)*	4.35 (2.82-6.18)
Baseline PSA density‡ (ng/ml^2)†	0.12 (0.10)
Age (years)*	62 (57-67)
Total number of PSA measurements	8262
Number of PSA measurements per patient*	9 (5-14)
PSA level (ng/ml)†	5.10 (3.84)
Number of core ratio per patient*	3 (2-4)
core ratio (%)*	8.33 (0.00-16.67)
Number of biopsies per patient*	2 (2-3)

* median is shown followed by the interval between 25% quantile and 75% quantile;
† mean is shown with standard deviation in the brackets;
‡: PSA density equals to PSA level (ng/ml) divided by prostate volume (ml).

Web Appendix A.2 Longitudinal Outcomes

In the Canary PASS data, two longitudinal outcome are available, namely, PSA levels and proportion of cores obtained by a biopsy that contain cancer cells (core ratio). In Web Figure 1, the development of the longitudinal outcomes is displayed for 20 randomly selected patients. The trajectories show non-linear evolutions over time, and vary greatly between patients, which needs to be accommodated in the longitudinal component of the ICJM.

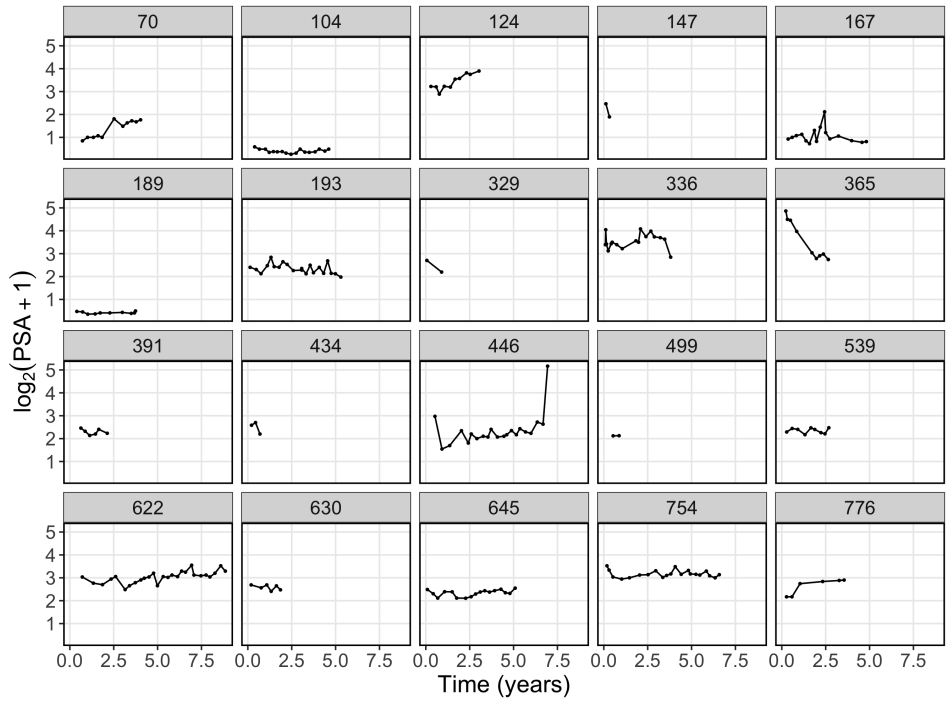

(a) PSA levels

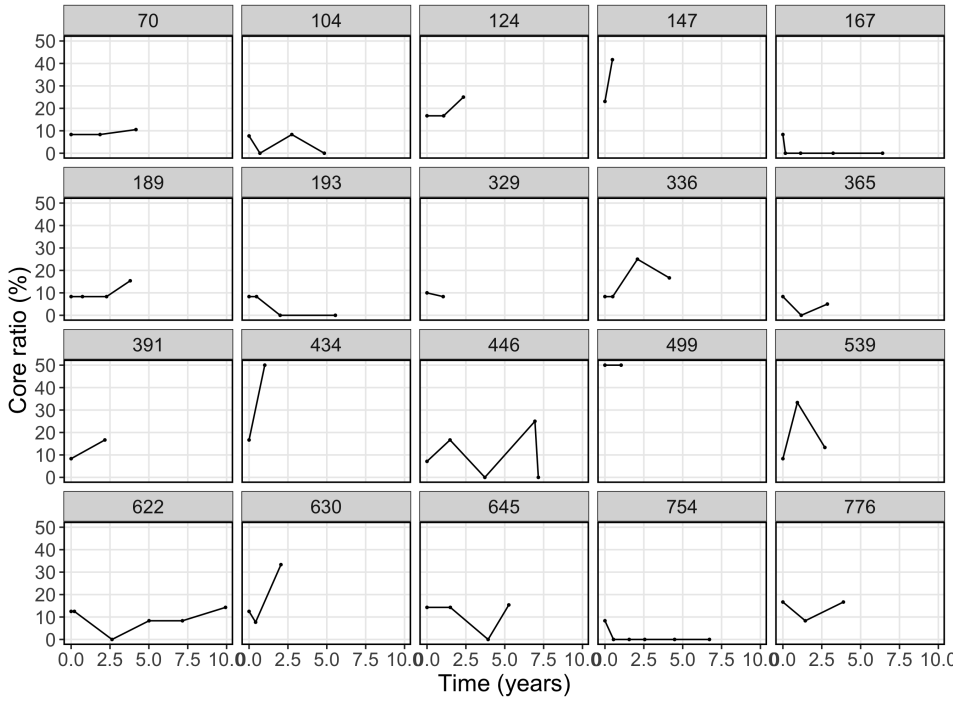

(b) Core ratios

Web Figure 1: Observed trajectories of two longitudinal outcomes for 20 randomly selected subjects.

Web Appendix B Interval-censored Cause-specific Joint Models (ICJM) for Longitudinal and Time-to-event Data

In the specification of the ICJM, we use a flexible semi-parametric specification of the baseline hazard using penalized B-splines,

$$\log h_0^{(k)}(t) = \gamma_{k,h_0,0} + \sum_{a=1}^{A} \gamma_{k,h_0,a} \mathcal{B}_a(t, \boldsymbol{\xi}),$$

where $\mathcal{B}_a(t, \boldsymbol{\xi})$ is the a-th basis function of a B-splines with knots $\xi_1, \ldots, \xi_A$. The number of knots was chosen to be 11. The penalized coefficients for the basis function $\boldsymbol{\gamma}_{k,h_0}$ have the following priors,

$$p(\boldsymbol{\gamma}_{k,h_0} \mid \tau_{k,h_0}) \propto \tau_{k,h_0}^{\rho(\boldsymbol{M})/2} \exp\left(-\frac{\tau_{k,h_0}}{2} \boldsymbol{\gamma}_{k,h_0}^\top \boldsymbol{M} \boldsymbol{\gamma}_{k,h_0}\right),$$

with

$$\tau_{k,h_0} \sim \text{Gamma}(5, 0.5),$$

where τ_{k,h_0} is the smoothing parameter; $\boldsymbol{M} = \Delta_r^\top \Delta_r + 10^{-6} I$, Δ_r is the r-th difference penalty matrix and $\rho(\boldsymbol{M})$ denotes the rank of $\boldsymbol{M}$.

Web Appendix C Simulation Study

Web Appendix C.1 Simulation Setting

To evaluate the performance of our proposed methodology, we simulated data based on the parameters from the ICJM fitted on the Canary PASS study (ICJM 1, see Section 5). The patients in the training sets are supposed to take biopsies in months 6, 12, 24 and afterwards biennially and PSA measurements every three months, with small variations.

This model had the following structure:

$$\begin{aligned}
\log_2(\text{PSA}_i + 1)(t) &= m_{1i}(t) + \epsilon_i(t), \\
m_{1i}(t) &= \beta_0 + b_{0i} + \sum_{p=1}^{3} (\beta_p + b_{pi}) \mathcal{C}_i^{(p)}(t) + \beta_4(\text{Age}_i - 62), \\
h_i^{(k)}\left\{t \mid \boldsymbol{\mathcal{M}}_{1i}(t)\right\} &= h_0^{(k)}(t) \exp\Big[\gamma_k \text{density}_i + f\left\{\boldsymbol{\mathcal{M}}_{1i}(t), \boldsymbol{\alpha}_k\right\}\Big],
\end{aligned}$$

where $\mathcal{C}(t)$is the design matrix for the natural cubic splines (with three degrees of freedom) for time t; Age_i and density_i refer to the patient's age and PSA density at the start of active surveillance, respectively. Baseline Age was centered by subtracting the median age (62 years) for computational reasons. Both the expected value of PSA and the change in expected PSA over the previous year were included as covariates in the time-to-event component, i.e.,

$$f\left\{\boldsymbol{\mathcal{M}}_{1i}(t), \boldsymbol{\alpha}_k\right\} = \alpha_{1k1} m_{1i}(t) + \alpha_{2k1}\Big\{m_{1i}(t) - m_{1i}(t-1)\Big\}.$$

The residuals of the longitudinal component were assumed to follow a student's t distribution with three degrees of freedom (Tomer et al., 2022),

$$\epsilon_i(t) \sim t(\frac{1}{\tau_\epsilon}, 3),$$

with

$$\tau_\epsilon \sim \text{Gamma}(0.01, 0.01).$$

The prior distributions for the regression coefficients were specified as vague normal distributions,

$$\begin{aligned}\beta &\sim \mathcal{N}(0, 100),\\ \gamma_k &\sim \mathcal{N}(0, 100),\\ \alpha &\sim \mathcal{N}(0, 100),\end{aligned}$$

and the variance-covariance matrix of the random effects, $\boldsymbol{D}$, to follow an inverse Wishart distribution,

$$\boldsymbol{D} \sim \mathcal{IW}(n_b + 1, \frac{4}{\tau_b}),$$

with

$$\tau_b \sim \text{Gamma}(0.5, 0.01),$$

where n_b is the number of coefficients for random effects.

The model was implemented in JAGS (Plummer, 2003) and run for 10000 iterations, using a thinning interval of 10, in each of three MCMC chains.

The resulting posterior means used for simulation were

$$\boldsymbol{\beta} = [2.34, 0.28, 0.61, 0.95, 0.02]^\top,$$

$$\boldsymbol{D} = \begin{bmatrix} 0.48 & -0.04 & -0.07 & 0.02 \\ -0.04 & 0.77 & 0.46 & -0.04 \\ -0.07 & 0.46 & 1.37 & 1.36 \\ 0.02 & -0.04 & 1.36 & 2.54 \end{bmatrix},$$

$$\tau_\epsilon = 47.40,$$

$$\boldsymbol{\gamma}_{h_0} = \begin{bmatrix} -6.78 & -5.76 \\ -4.72 & -4.99 \\ -2.84 & -4.43 \\ -1.65 & -4.26 \\ -1.54 & -4.36 \\ -1.79 & -4.47 \\ -1.85 & -4.60 \\ -1.75 & -4.69 \\ -1.85 & -4.78 \\ -2.04 & -4.92 \\ -2.18 & -5.08 \\ -2.32 & -5.21 \end{bmatrix},$$

$$\boldsymbol{\gamma} = [0.50, 0.23],$$

$$\boldsymbol{\alpha} = \begin{bmatrix} 0.13 & 0.42 \\ 3.01 & 2.62 \end{bmatrix}.$$

The resulting simulated data matched the observed data well with regard to the rates of cancer progression, early treatment initiation and censoring (Web Table 2).

Web Table 2: Summary of event proportions in the simulated training datasets compared to the observed data.

Events	**Simulated data**† (%)	**Observed data** (%)
Cancer progression	28.21	21.97
Treatment	8.36	10.44
Censoring	63.43	67.59

†: the average proportions overall training sets are presented.

Web Appendix C.2 Evaluation of the ICJM

Since the quality of the personalized schedules relies on good predictive accuracy, we investigated the prediction error of the ICJM.

We predicted the 2-year cancer progression risk at different starting points (baseline, year 1, 2, 3, 4 and 6) for all patients in the test sets based on the ICJMs fitted on the corresponding training sets and calculated the prediction error (i.e., the difference between the true and predicted risk) in R (**?**).

Web Figure 2 visualizes these results; it shows that the ICJM slightly overestimates the 2-year progression risk for later years. Further investigation revealed that this likely stems

from the overestimation of the baseline hazard, as shown in Web Figure 3. The placement of the knots in the spline specification of the baseline hazard is based on the quantiles of the event times in the training data. Since most events occur between years 3 and 4, there is little information to guide the spline fit in the period after year 5.

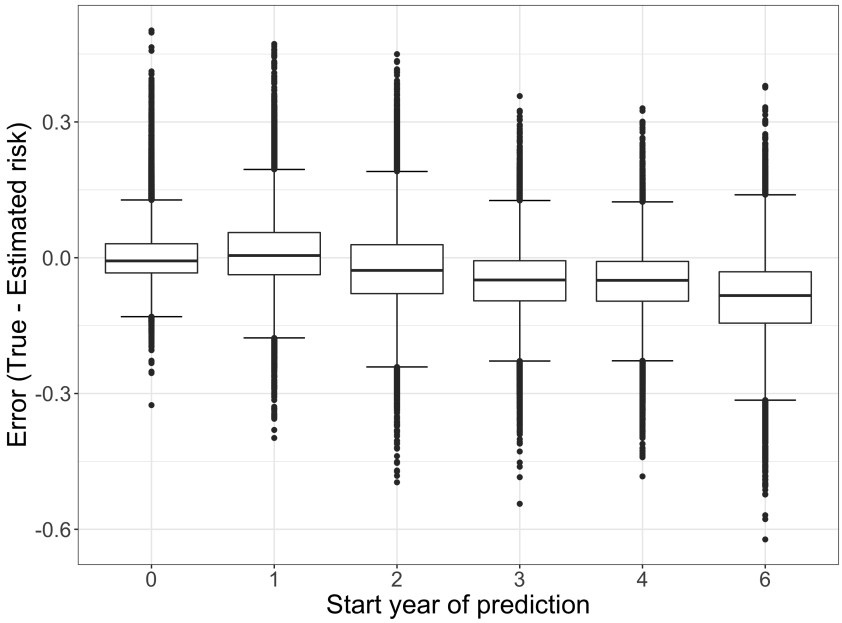

Web Figure 2: Two-year risk prediction performance evaluation for 200 test sets.

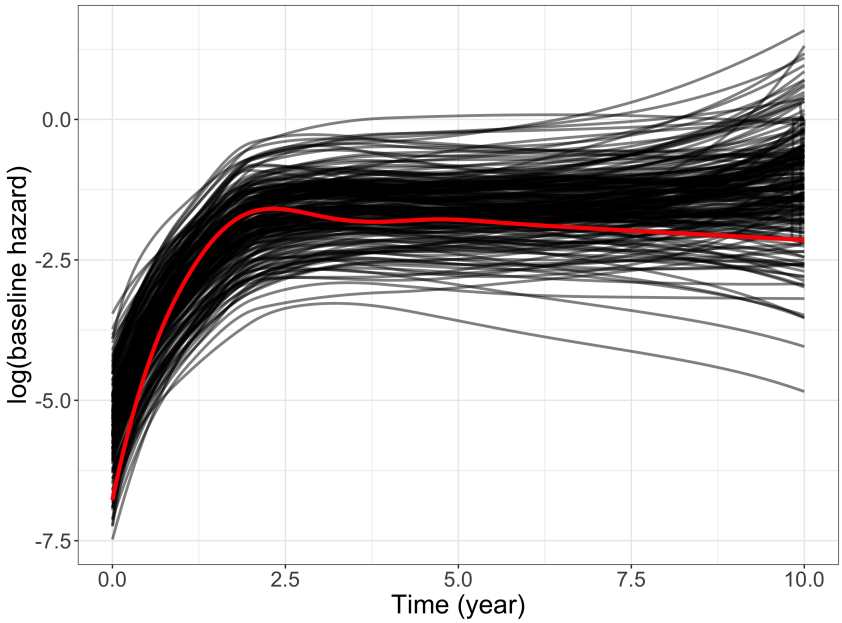

Web Figure 3: Visualization of the baseline hazards over time (red curve: true baseline hazard ; black curves: estimated baseline hazards).

Web Appendix D ICJM for Data Analysis

The model specification of our primary model, ICJM 1, is detailed in Web Appendix C.1.

Web Appendix D.1 Model Specification of ICJM 2

To investigate the role of the core ratio as a potential predictor for cancer progression and to demonstrate how to incorporate additional biomarkers in the ICJM, we extended ICJM with a binomial mixed model for the core ratio. In this model, we assumed a quadratic evolution over time. The random effects were modelled jointly with the random effects in the model for PSA, i.e.,

$$\begin{aligned}
\log_2(\text{PSA}_i + 1)(t) &= m_{1i}(t) + \epsilon_i(t), \\
m_{1i}(t) &= \beta_0 + b_{0i} + \sum_p^3 (\beta_p + b_{pi}) \mathcal{C}_i^{(p)}(t) + \beta_4(\text{Age}_i - 62), \\
E\left[\text{logit}\left\{\text{core-ratio}_i(t)\right\}\right] &= m_{2i}(t), \\
m_{2i}(t) &= \beta_5 + b_{4i} + (\beta_6 + b_{5i})t + (\beta_7 + b_{6i})t^2,
\end{aligned}$$

where the random effects from the two longitudinal outcomes $\boldsymbol{b}_i = (b_{1i}, \ldots, b_{6i})^\top$ are modeled jointly using a multivariate normal distribution, $\boldsymbol{b}_i \sim \mathcal{N}(0, \boldsymbol{D})$.

The survival component of the ICJM was extended to also include the estimated trajec-

tory of the core-ratio, $\boldsymbol{\mathcal{M}}_{2i}(t)$,

$$h_i^{(k)}\left\{t \mid \boldsymbol{\mathcal{M}}_{1i}(t), \boldsymbol{\mathcal{M}}_{2i}(t)\right\} = h_0^{(k)}(t) \exp\Big[\gamma_k \text{density}_i + f\left\{\boldsymbol{\mathcal{M}}_{1i}(t), \boldsymbol{\mathcal{M}}_{2i}(t), \boldsymbol{\alpha}_k\right\}\Big],$$

where $\boldsymbol{\alpha}_k = [\alpha_{11k}, \alpha_{12k}, \alpha_{2k}]$ and $f\left\{\boldsymbol{\mathcal{M}}_{1i}(t), \boldsymbol{\mathcal{M}}_{2i}(t), \boldsymbol{\alpha}_k\right\}$ now also included the expected value of the core ratio,

$$\begin{aligned} f\left\{\boldsymbol{\mathcal{M}}_{1i}(t), \boldsymbol{\mathcal{M}}_{2i}(t), \boldsymbol{\alpha}_k\right\} = \alpha_{1k1} m_{1i}(t) + \alpha_{2k1}\Big\{m_{1i}(t) - m_{1i}(t-1)\Big\} \\ + \alpha_{1k2} m_{2i}(t). \end{aligned}$$

ICJM 2 was fitted in JAGS, using 10000 iterations, using a thinning interval of 10, in each of three MCMC chains.

Web Appendix D.2 Goodness of fit

The goodness of fit the ICJM depends on the fit of individual expected trajectories of the biomarkers. Therefore, we examined the fitted trajectories of PSA levels and core ratios for the 20 selected subjects in Web Figure 1. The results are visualized in Web Figure 4. It is shown that the ICJM is able to generally capture the non-linear trends for the biomarkers of each individual patient.

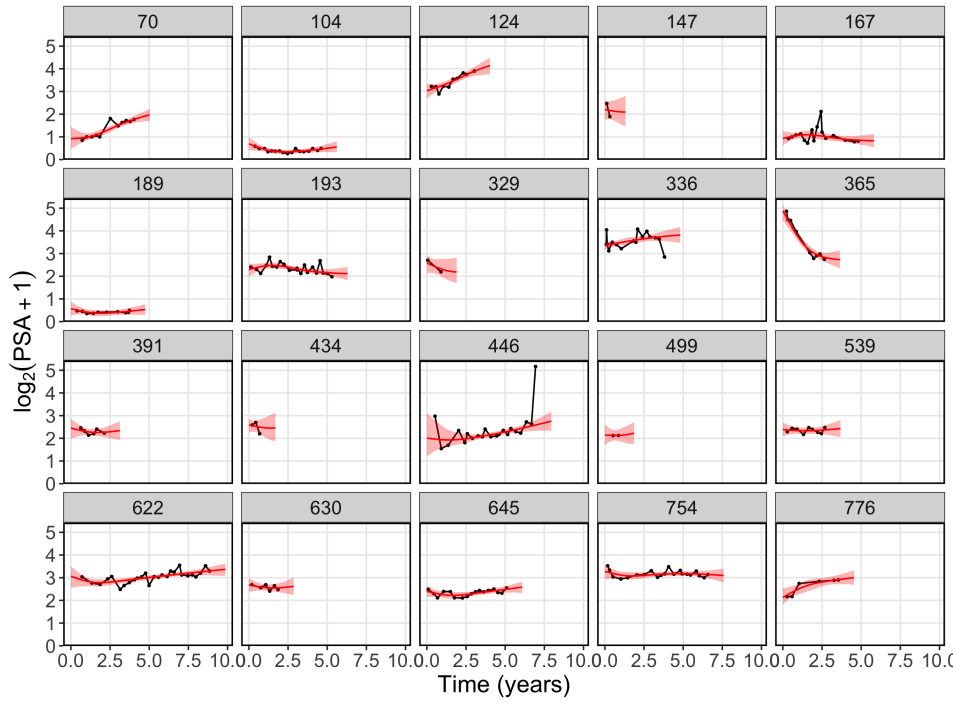

(a) PSA levels

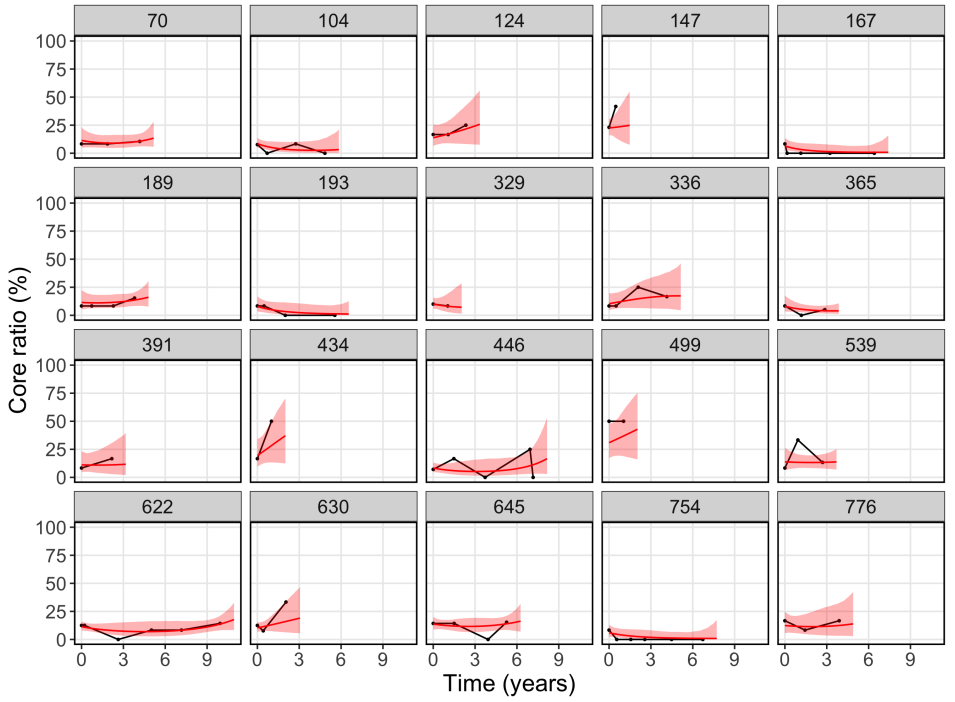

(b) Core ratios

Web Figure 4: Fitted trajectories of two longitudinal outcomes for 20 randomly selected subjects.

Web Appendix D.3 Results

The results from ICJM 1 and ICJM 2 are presented in Web Table 3. Since the coefficients pertaining to the natural cubic splines used to model the non-linearity of the trajectories of the PSA levels do not have a direct and clinically meaningful interpretation and to facilitate the interpretation, we present effect plots of the estimated PSA level trajectory and core ratio trajectory for patients with the median age of 62 years in Web Figure 5. Both outcomes remained stable at the beginning and increased with time.

Web Table 3: Summary of the model parameter estimates in ICJM 1 and ICJM 2.

Parameters	**ICJM 1 (PSA)**		**ICJM 2 (PSA + core ratio)**	
	Estimate	**95% CI**	**Estimate**	**95% CI**
Longitudinal component - PSA				
Intercept	2.34	[2.29, 2.39]	2.34	[2.30, 2.39]
Time 1†	0.28	[0.19, 0.39]	0.31	[0.22, 0.39]
Time 2†	0.61	[0.40, 0.82]	0.63	[0.45, 0.81]
Time 3†	0.95	[0.60, 1.34]	0.99	[0.70, 1.30]
Age	0.02	[0.01, 0.02]	0.02	[0.01, 0.02]
Longitudinal component - core ratio				
Intercept	-	-	-2.08	[-2.14, -2.03]
Time	-	-	-0.20	[-0.27, -0.12]
Time^2	-	-	0.04	[0.02, 0.05]
Progression-specific survival component				
log(PSA density)	0.50	[0.24, 0.76]	0.32	[0.02, 0.62]
$\log_2(\text{PSA}+1)$ value	0.13	[-0.09, 0.34]	0.23	[-0.02, 0.47]
$\log_2(\text{PSA}+1)$ yearly change	3.01	[1.83, 4.19]	1.92	[0.56, 3.17]
logit[E(core ratio)] value	-	-	1.16	[0.96, 1.36]
Treatment-specific survival component				
log(PSA density)	0.23	[-0.20, 0.66]	-0.36	[-0.95, 0.22]
$\log_2(\text{PSA}+1)$ value	0.42	[0.10, 0.74]	0.63	[0.20, 1.10]
$\log_2(\text{PSA}+1)$ yearly change	2.62	[0.62, 4.69]	2.07	[-0.54, 4.67]
logit[E(core ratio)] value	-	-	1.84	[1.44, 2.32]

† Time variable is specified in natural cubic splines with 3 degrees of freedom;

Note: CI: credible interval

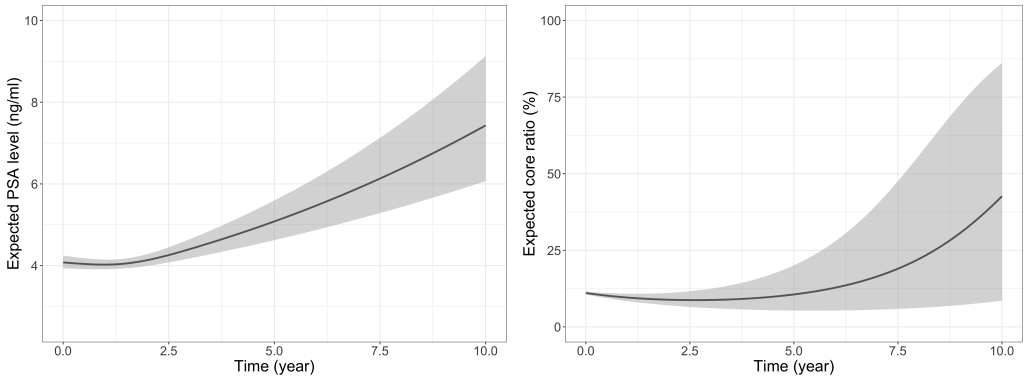

(a) (b)

Web Figure 5: Effect of time in the longitudinal modeling of (a) the PSA level and (b) the core ratio (ICJM 2).

The estimated effect of the core ratio is visualized in Web Figure 6. A one-fold increase of the core ratio to 30% raised the progression-specific risk by a factor of 8.40 times while halving the core ratio lowered the risk by 59%.

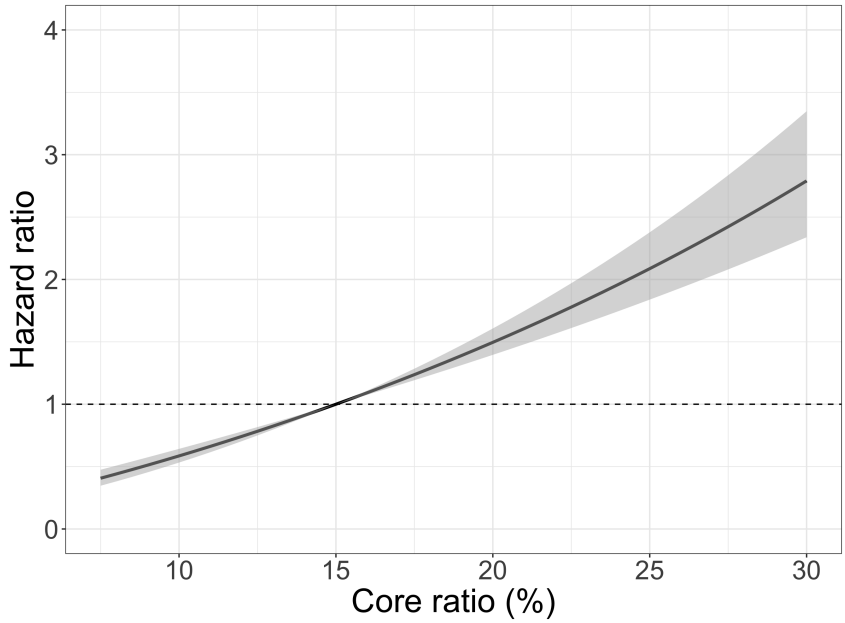

Web Figure 6: Effect of the core ratio value (contrast to a core ratio of 15%) on the risk of progression, considering the baseline PSA density, the current PSA level and PSA magnitude of change over the past year remain constant.

References

Adamy, A., Yee, D. S., Matsushita, K., Maschino, A., Cronin, A., Vickers, A., Guillonneau, B., Scardino, P. T., and Eastham, J. A. (2011). Role of prostate specific antigen and immediate confirmatory biopsy in predicting progression during active surveillance for low risk prostate cancer. *The Journal of Urology* **185,** 477–482.

Aizer, A. A., Gu, X., Chen, M.-H., Choueiri, T. K., Martin, N. E., Efstathiou, J. A., Hyatt, A. S., Graham, P. L., Trinh, Q.-D., Hu, J. C., and Nguyen, P. L. (2015). Cost implications and complications of overtreatment of low-risk prostate cancer in the United States. *Journal of the National Comprehensive Cancer Network* **13,** 61–68.

Albertsen, P. C., Hanley, J. A., and Fine, J. (2005). 20-year outcomes following conservative management of clinically localized prostate cancer. *JAMA* **293,** 2095–2101.

Andrinopoulou, E.-R. and Rizopoulos, D. (2016). Bayesian shrinkage approach for a joint model of longitudinal and survival outcomes assuming different association structures. *Statistics in Medicine* **35,** 4813–4823.

Bruinsma, S. M., Bokhorst, L. P., Roobol, M. J., and Bangma, C. H. (2016). How often is biopsy necessary in patients with prostate cancer on active surveillance? *Journal of Urology* **195,** 11–12.

Bul, M., Zhu, X., Valdagni, R., Pickles, T., Kakehi, Y., Rannikko, A., Bjartell, A., Van Der Schoot, D. K., Cornel, E. B., Conti, G. N., Boevé, E. R., Staerman, F., Vis-Maters, J. J., Vergunst, H., Jaspars, J. J., Strölin, P., Van Muilekom, E., Schröder, F. H., Bangma, C. H., and Roobol, M. J. (2013). Active surveillance for low-risk prostate cancer worldwide: the PRIAS study. *European Urology* **63,** 597–603.

Cary, K. C. and Cooperberg, M. R. (2013). Biomarkers in prostate cancer surveillance and screening: past, present, and future. *Therapeutic Advances in Urology* **5,** 318–329.

Chen, R. C., Rumble, R. B., Loblaw, D. A., Finelli, A., Ehdaie, B., Cooperberg, M. R., Morgan, S. C., Tyldesley, S., Haluschak, J. J., Tan, W., Justman, S., and Jain, S. (2016). Active surveillance for the management of localized prostate cancer (Cancer Care Ontario Guideline): American Society of Clinical Oncology clinical practice guideline endorsement. *Journal of Clinical Oncology: Official Journal of the American Society of Clinical Oncology* **34,** 2182–2190.

Cooperberg, M. R., Zheng, Y., Faino, A. V., Newcomb, L. F., Zhu, K., Cowan, J. E., Brooks, J. D., Dash, A., Gleave, M. E., Martin, F., Morgan, T. M., Nelson, P. S., Thompson, I. M., Wagner, A. A., Carroll, P. R., and Lin, D. W. (2020). Tailoring intensity of active surveillance for low-risk prostate cancer based on individualized prediction of risk stability. *JAMA Oncology* **6,** e203187–e203187.

Dall'Era, M. A., Cooperberg, M. R., Chan, J. M., Davies, B. J., Albertsen, P. C., Klotz, L. H., Warlick, C. A., Holmberg, L., Bailey Jr, D. E., Wallace, M. E., Kantoff, P. W., and Carroll, P. R. (2008). Active surveillance for early-stage prostate cancer. *Cancer* **112,** 1650–1659.

Davis, J. W., Ward, J. F. r., Pettaway, C. A., Wang, X., Kuban, D., Frank, S. J., Lee, A. K., Pisters, L. L., Matin, S. F., Shah, J. B., Karam, J. A., Chapin, B. F., Papadopoulos,

J. N., Achim, M., Hoffman, K. E., Pugh, T. J., Choi, S., Troncoso, P., Logothetis, C. J., and Kim, J. (2016). Disease reclassification risk with stringent criteria and frequent monitoring in men with favourable-risk prostate cancer undergoing active surveillance. *BJU International* **118,** 68–76.

De Carvalho, T. M., Heijnsdijk, E. A., and De Koning, H. J. (2017). Estimating the risks and benefits of active surveillance protocols for prostate cancer: a microsimulation study. *BJU International* **119,** 560–566.

Eminaga, O., Shkolyar, E., Breil, B., Semjonow, A., Boegemann, M., Xing, L., Tinay, I., and Liao, J. C. (2022). Artificial intelligence-based prognostic model for urologic cancers: a SEER-based study. *Cancers* **14,**.

Gandaglia, G., Leni, R., Bray, F., Fleshner, N., Freedland, S. J., Kibel, A., Stattin, P., Van Poppel, H., and La Vecchia, C. (2021). Epidemiology and prevention of prostate cancer. *European Urology Oncology* **4,** 877–892.

Garthwaite, P. H., Fan, Y., and Sisson, S. A. (2016). Adaptive optimal scaling of Metropolis–Hastings algorithms using the Robbins–Monro process. *Communications in Statistics - Theory and Methods* **45,** 5098–5111.

Godtman, R. A., Holmberg, E., Khatami, A., Pihl, C.-G., Stranne, J., and Hugosson, J. (2016). Long-term results of active surveillance in the Göteborg randomized, population-based prostate cancer screening trial. *European Urology* **70,** 760–766.

Ishwaran, H., Kogalur, U. B., Blackstone, E. H., and Lauer, M. S. (2008). Random survival forests. *The Annals of Applied Statistics* **2,** 841 – 860.

Klotz, L., Vesprini, D., Sethukavalan, P., Jethava, V., Zhang, L., Jain, S., Yamamoto, T., Mamedov, A., and Loblaw, A. (2015). Long-term follow-up of a large active surveillance cohort of patients with prostate cancer. *Journal of Clinical Oncology : Official Journal of the American Society of Clinical Oncology* **33,** 272–277.

Lee, C., Light, A., Saveliev, E. S., Van der Schaar, M., and Gnanapragasam, V. J. (2022). Developing machine learning algorithms for dynamic estimation of progression during active surveillance for prostate cancer. *npj Digital Medicine* **5,** 110.

Lowenstein, L. M., Basourakos, S. P., Williams, M. D., Troncoso, P., Gregg, J. R., Thompson, T. C., and Kim, J. (2019). Active surveillance for prostate and thyroid cancers: evolution in clinical paradigms and lessons learned. *Nature Reviews. Clinical Oncology* **16,** 168–184.

Mamawala, M. M., Rao, K., Landis, P., Epstein, J. I., Trock, B. J., Tosoian, J. J., Pienta, K. J., and Carter, H. B. (2017). Risk prediction tool for grade re-classification in men with favourable-risk prostate cancer on active surveillance. *BJU International* **120,** 25–31.

Nayan, M., Salari, K., Bozzo, A., Ganglberger, W., Lu, G., Carvalho, F., Gusev, A., Schneider, A., Westover, B. M., and Feldman, A. S. (2022). A machine learning approach to predict progression on active surveillance for prostate cancer. *Urologic Oncology: Seminars and Original Investigations* **40,** 161.e1–161.e7.

Nelson, T. J., Javier-DesLoges, J., Deka, R., Courtney, P. T., Nalawade, V., Mell, L., Murphy, J., Parsons, J. K., and Rose, B. S. (2021). Association of prostate-specific antigen velocity with clinical progression among African American and non-Hispanic white men treated for low-risk prostate cancer with active surveillance. *JAMA Network Open* **4,** e219452–e219452.

Newcomb, L. F., Thompson, I. M. J., Boyer, H. D., Brooks, J. D., Carroll, P. R., Cooperberg, M. R., Dash, A., Ellis, W. J., Fazli, L., Feng, Z., Gleave, M. E., Kunju, P., Lance, R. S., McKenney, J. K., Meng, M. V., Nicolas, M. M., Sanda, M. G., Simko, J., So, A., Tretiakova, M. S., Troyer, D. A., True, L. D., Vakar-Lopez, F., Virgin, J., Wagner, A. A., Wei, J. T., Zheng, Y., Nelson, P. S., and Lin, D. W. (2016). Outcomes of active surveillance for clinically localized prostate cancer in the prospective, multi-institutional Canary PASS cohort. *The Journal of Urology* **195,** 313–320.

Pearson, J. D., Morrell, C. H., Landis, P. K., Carter, H. B., and Brant, L. J. (1994). Mixed-effects regression models for studying the natural history of prostate disease. *Statistics in Medicine* **13,** 587–601.

Pernar, C. H., Ebot, E. M., Wilson, K. M., and Mucci, L. A. (2018). The epidemiology of prostate cancer. *Cold Spring Harbor Perspectives in Medicine* **8,** a030361.

Plummer, M. (2003). JAGS: a program for analysis of bayesian graphical models using Gibbs sampling. In Hornik, K., Leisch, F., and Zeileis, A., editors, *Proceedings of the 3rd International Workshop on Distributed Statistical Computing (DSC 2003)*. ISSN: 1609-395X.

Rizopoulos, D. (2011). Dynamic predictions and prospective accuracy in joint models for longitudinal and time-to-event data. *Biometrics* **67,** 819–829.

Schuster, N. A., Hoogendijk, E. O., Kok, A. A., Twisk, J. W., and Heymans, M. W. (2020). Ignoring competing events in the analysis of survival data may lead to biased results: a nonmathematical illustration of competing risk analysis. *Journal of Clinical Epidemiology* **122,** 42–48.

Selvadurai, E. D., Singhera, M., Thomas, K., Mohammed, K., Woode-Amissah, R., Horwich, A., Huddart, R. A., Dearnaley, D. P., and Parker, C. C. (2013). Medium-term outcomes of active surveillance for localised prostate cancer. *European Urology* **64,** 981–987.

Tomer, A., Nieboer, D., Roobol, M. J., Steyerberg, E. W., and Rizopoulos, D. (2019). Personalized schedules for surveillance of low-risk prostate cancer patients. *Biometrics* **75,** 153–162.

Tomer, A., Nieboer, D., Roobol, M. J., Steyerberg, E. W., and Rizopoulos, D. (2022). Shared decision making of burdensome surveillance tests using personalized schedules and their burden and benefit. *Statistics in Medicine* **41,** 2115–2131.

Tosoian, J. J., Trock, B. J., Landis, P., Feng, Z., Epstein, J. I., Partin, A. W., Walsh, P. C., and Carter, H. B. (2011). Active surveillance program for prostate cancer: an update of the Johns Hopkins experience. *Journal of Clinical Oncology: Official Journal of the American Society of Clinical Oncology* **29,** 2185–2190.

Welty, C. J., Cowan, J. E., Nguyen, H., Shinohara, K., Perez, N., Greene, K. L., Chan, J. M., Meng, M. V., Simko, J. P., Cooperberg, M. R., and Carroll, P. R. (2015). Extended followup and risk factors for disease reclassification in a large active surveillance cohort for localized prostate cancer. *The Journal of Urology* **193,** 807–811.

Whittemore, A. S., Wu, A. H., Kolonel, L. N., John, E. M., Gallagher, R. P., Howe, G. R., West, D. W., Teh, C.-Z., and Stamey, T. (1995). Family history and prostate cancer risk in black, white, and asian men in the United States and Canada. *American Journal of Epidemiology* **141,** 732–740.

Zhou, G.-Q., Wu, C.-F., Deng, B., Gao, T.-S., Lv, J.-W., Lin, L., Chen, F.-p., Kou, J., Zhang, Z.-X., Huang, X.-D., Zheng, Z.-Q., Ma, J., Liang, J.-H., and Sun, Y. (2020). An optimal posttreatment surveillance strategy for cancer survivors based on an individualized risk-based approach. *Nature Communications* **11,** 3872.